Electromagnetics
Publication details, including instructions for authors and subscription information:
http://www.tandfonline.com/loi/uemg20

An Investigation of a Preconditioner for High-Frequency Maxwell Problems

P. D. Ledger [a]
[a] Civil and Computational Engineering Research Centre, School of Engineering, Swansea University , Swansea, UK
Published online: 08 Mar 2010.

To cite this article: P. D. Ledger (2010) An Investigation of a Preconditioner for High-Frequency Maxwell Problems, Electromagnetics, 30:1-2, 94-126, DOI: 10.1080/02726340903485364

To link to this article: http://dx.doi.org/10.1080/02726340903485364

Electromagnetics, 30:94–126, 2010

ISSN: 0272-6343 print/1532-527X online
DOI: 10.1080/02726340903485364

Taylor & Francis
Taylor & Francis Group

An Investigation of a Preconditioner for High-Frequency Maxwell Problems

P. D. LEDGER[1]

[1]Civil and Computational Engineering Research Centre,
School of Engineering, Swansea University, Swansea, UK

Abstract *This article describes a preconditioner for the indefinite linear equation system that is obtained when the vector wave equation is discretized by hp edge finite elements. A theoretical investigation of the eigenspectrum of the preconditioned system for p = 1 quadrilateral elements illustrates that the preconditioner will perform well, once the mesh spacing is sufficiently fine. Numerical experiments are included, which demonstrate the effectiveness of the preconditioner for h and p refinements in both two and three dimensions.*

Keywords electromagnetic wave propagation, *hp* finite elements, efficient preconditioning

1. Introduction

This work addresses problems where the time harmonic electric field $\boldsymbol{E}$ satisfies the vector wave equation

$$curl\, \mu^{-1} curl\, \boldsymbol{E} + \kappa \boldsymbol{E} = \boldsymbol{0} \tag{1}$$

in a bounded domain $\Omega \subset \mathbb{R}^3$ or $\Omega \subset \mathbb{R}^2$. On the boundaries of this domain, suitable Dirichlet- or Neumann-type data is supplied. The materials considered are such that the permeability μ and permittivity ϵ are isotropic and homogeneous.[1] The regime of interest is restricted to high-frequency problems where $\kappa = -\omega^2\epsilon$, and ω is the angular frequency. With these assumptions, $\mu > 0$, $\epsilon > 0$, and $\kappa < 0$ are scalar constants. A finite element approximation to this problem is explored, addressing, in particular, issues related to the efficient solution of the linear system.

The use of edge elements for the finite element approximation of problems in electromagnetism is now well established. This special type of finite element owes its name to the fact that, in the lowest order case, it approximates the tangential component of the field as a constant on each edge. The edge finite element was originally introduced by Nédélec (1978, 1980, 1986). Edge elements are often known under alternative names;

Received 1 November 2008; accepted 8 May 2009.

[1]Note that the finite element method used is also applicable to more general materials; however, these simplifications are necessary for the mathematical analysis presented in Section 3.

Address correspondence to P. D. Ledger, Civil and Computational Engineering Research Centre, School of Engineering, University of Wales Swansea, Swansea SA2 8PP, United Kingdom. E-mail: P.D.Ledger@swansea.ac.uk

some engineers prefer to call them vector finite elements, while mathematicians usually prefer to call them $\boldsymbol{H}(curl)$-conforming finite elements. Henceforth, the latter of these names will be adopted. Incidentally, the space $\boldsymbol{H}(curl)$ provides the correct mathematical setting for solving the vector wave equation (Eq. (1)); therefore, it is natural that one should use finite elements that conform to this space to obtain a discrete approximation for $\boldsymbol{E}$. Within the engineering literature, the focus in the past has been on applying low-order versions of $\boldsymbol{H}(curl)$-conforming elements to practical problems; for details, see (Ledger & Morgan, 2005) and the references therein. This type of element has become very popular among engineers due to its ability to correctly capture material interfaces and the ease in which boundary conditions can be incorporated. Unfortunately, for high-frequency problems, the poor dispersive properties of low-order $\boldsymbol{H}(curl)$-conforming elements (Ainsworth, 2004) lead to the requirement for meshes with large numbers of elements in order to resolve the short wavelengths involved (El hachemi et al., 2004).

In recent years, there has been growing interest in the ability that higher-order versions of these elements have to accurately capture electromagnetic fields. In this respect, the *hp* finite element method (Schwab, 1998) has attracted particular attention, as it offers the possibility of combining an arbitrarily high polynomial degree (p) for capturing smooth features of the solution with local mesh (h) refinement for localizing the effects of singularities at sharp corners and material interfaces. An *hp* extension of $\boldsymbol{H}(curl)$-conforming elements was first developed by Demkowicz and Rachowicz (1998) and Demkowicz and Vardapetyan (1998) and was applied to hybrid meshes of triangles and quadrilaterals in two dimensions and, later, to structured meshes of hexahedra in three dimensions (Rachowicz & Demkowicz, 2002). Ainsworth and Coyle (2003b) developed new sets of basis functions for the *hp* version of $\boldsymbol{H}(curl)$-conforming elements for hybrid meshes of triangles and quadrilaterals in two dimensions (Ainsworth & Coyle, 2001) and unstructured meshes of tetrahedra in three dimensions. These elements have been successfully applied to electromagnetic scattering problems (Ledger, 2002; Ledger & Morgan, 2005; Ledger et al., 2002, 2003, 2004, 2007) as well as other applications (Coyle & Ledger, 2004; Ainsworth et al., 2003; Ledger & Morgan, 2005).

Schöberl and Zaglmayr (2005) developed an alternative set of basis functions for the *hp* version of $\boldsymbol{H}(curl)$-conforming elements for hybrid meshes of triangles and quadrilaterals in two dimensions and hybrid meshes of tetrahedra, prisms, pyramids, and hexahedra in three dimensions. The construction of their elements is based on the fact that the space $\boldsymbol{H}(curl)$ forms part of the DeRham sequence

$$H^1 \xrightarrow{\nabla} \boldsymbol{H}(curl) \xrightarrow{curl} \boldsymbol{H}(\mathrm{div}) \xrightarrow{\mathrm{div}} L^2,$$

in three dimensions (Monk, 2003). The spaces $\boldsymbol{H}(curl)$ and $\boldsymbol{H}(\mathrm{div})$ also satisfy a similar set of two shortened sequences in two dimensions (Zaglmayr, 2006). The definitions of $\boldsymbol{H}(curl)$ and $\boldsymbol{H}(\mathrm{div})$ are

$$\boldsymbol{H}(curl) = \{\boldsymbol{v} | \boldsymbol{v} \in (L_2)^d, curl\, \boldsymbol{v} \in (L_2)^{2d-3}\},$$

$$\boldsymbol{H}(\mathrm{div}) = \{\boldsymbol{v} | \boldsymbol{v} \in (L_2)^d, \mathrm{div}\, \boldsymbol{v} \in L_2\},$$

where $d = 2, 3$ is the number of dimensions of the problem. Schöberl and Zaglmayr's elements are special in that the construction of their basis functions explicitly follow

the DeRham sequence. For example, their $\boldsymbol{H}(curl)$-conforming basis functions explicitly contain gradients of the basis functions for H^1 functions, their $\boldsymbol{H}(\mathrm{div})$-conforming basis functions explicitly contain the curl of their $\boldsymbol{H}(curl)$-conforming basis functions, and their L^2-conforming functions explicitly contain the divergence of their $\boldsymbol{H}(curl)$-conforming basis functions. For three-dimensional elements, the global space for their $\boldsymbol{H}(curl)$-conforming discretization can be decomposed as

$$V_p = V_{\mathcal{N}_0} + \sum_{E_i} V_{E_i}^p + \sum_{F_i} V_{F_i}^p + \sum_{I_i} V_{I_i}^p \subset \boldsymbol{H}(curl),$$

where the subscripts $\mathcal{N}_0$, E, F, and I refer to the parts of the discretization given by the lowest-order ($p = 0$) edge functions, higher-order ($p > 0$) edge functions, face functions, and interior functions, respectively. The corresponding global space for their H^1-conforming discretization can be decomposed as

$$W_{p+1} = W_V + \sum_{E_i} W_{E_i}^{p+1} + \sum_{F_i} W_{F_i}^{p+1} + \sum_{I_i} W_{I_i}^{p+1} \subset H^1,$$

where the subscripts V, E, F, and I refer to the parts of the discretization given by the lowest-order vertex functions ($p = 1$), higher-order edge functions ($p > 1$), face functions, and interior functions, respectively. For triangles and quadrilaterals in two dimensions, similar decompositions apply (Zaglmayr, 2006). The DeRham complex is fulfilled by choosing

$$\nabla W_V \subset V_{\mathcal{N}_0}, \qquad \nabla W_{E_i}^{p+1} = V_{E_i}^p, \qquad \nabla W_{F_i}^{p+1} \subset V_{F_i}^p, \qquad \nabla W_{I_i}^{p+1} \subset V_{I_i}^p.$$

Returning to the problem introduced in Eq. (1), note that the usual first step in a finite element approximation is to write down the weak variational problem, which in this case is (e.g., Ledger, 2002): Find $\boldsymbol{E} \in \boldsymbol{H}(curl)$ such that

$$k(\boldsymbol{E}, \boldsymbol{w})_\Omega = \ell(\boldsymbol{w}) \qquad \forall \boldsymbol{w} \in \boldsymbol{H}(curl), \tag{2}$$

where

$$k(\boldsymbol{E}, \boldsymbol{w})_\Omega = (\mu^{-1} curl\, \boldsymbol{E}, curl\, \boldsymbol{w})_\Omega + (\kappa \boldsymbol{E}, \boldsymbol{w})_\Omega,$$

$$\ell(\boldsymbol{w}) = -\int_{\partial\Omega} \boldsymbol{w} \cdot \boldsymbol{n} \times curl\, \boldsymbol{E}\, \mathrm{d}s,$$

and $(\boldsymbol{u}, \boldsymbol{v})_\Omega = \int_\Omega \boldsymbol{u} \cdot \boldsymbol{v} \mathrm{d}\Omega$. The vector $\boldsymbol{n}$ is the outward normal to $\partial\Omega$. It is well known that the Galerkin finite element discretization of this variational statement (using either low-order or hp version $\boldsymbol{H}(curl)$-conforming finite elements) yields the linear system of equations

$$Kx = r, \tag{3}$$

where, for the problems under consideration, K is a sparse $n \times n$ symmetric system matrix, x is a column vector of unknowns, and r is a known column vector. The matrix K has the property that $x^T K x > 0$ or $x^T K x < 0$, depending on x, which means that K is indefinite with both positive and negative real eigenvalues.

As K is indefinite, this rules out the use of certain iterative techniques, such as the conjugate gradient algorithm, for the solution of the (unpreconditioned) system.[2] The indefinite nature of the matrix limits the choice of iterative solution technique to those that can cope with matrices with both positive and negative eigenvalues; the quasi minimum residual (QMR), generalized minimum residual (GMRES), and variants of biconjugate gradient (BICG) algorithms are possible candidates. Despite these methods being suitable for indefinite matrices, they may be slow to converge for large practical problems without a suitable preconditioner C^{-1}. Algorithmic details for preconditioned versions of GMRES, QMR, and BICG can be found in standard texts books (e.g., Saad, 1996; Golub & Van Loan, 1996).

One of the earliest successful preconditioned iterative strategies for the solution of wave propagation problems was presented by Bayliss et al. (1983). Their focus was the scalar Helmholtz equation at low frequencies, and for this problem, they described an iterative approach based on the conjugate gradient algorithm with a Laplace preconditioner applied to the normal equations. Since this early pioneering work, a large number of alternative schemes have been presented, and following Erlangga et al. (2005), these can be identified as being a member of one of two classes. A nonexhaustive survey of recent preconditioning approaches is given below; further alternatives can also be found within the references quoted.

The first class of preconditioners are called "matrix based," as they are chosen in such a way that C^{-1} approximates the inverse of K. Examples of this class of preconditioners include those based on an incomplete LU (ILU) decomposition of K or on an approximate inverse of K. Preconditioners of this kind have been investigated for both the Helmholtz equation (e.g., Monga Made, 2001), as well as the vector wave equation (e.g., Chinellato, 2005), and although the effort required for a single iteration may be relatively cheap, the storage requirements of the decomposition may exceed those of K. Furthermore, the ILU decomposition may not be stable, as K is not a M matrix (Saad, 1996).

The second class of preconditioners are those that are "operator based." These are built based on an operator for which the spectrum of $C^{-1}K$ is favorably clustered. An interesting feature of this type of preconditioner is that the operator does not necessarily have to be an inverse of the Helmholtz (or the vector wave) operator. For the Helmholtz equation, approaches include the Laplace preconditioner (Bayliss et al., 1983), and later enhancements were achieved by adding positive zero-order terms (Laird & Giles, 2002) or complex-valued zero-order terms (Erlangga et al., 2004, 2005, 2006). The operator based preconditioner (for the Helmholtz equation) is usually applied approximately by an ILU-type decomposition or a multi-grid scheme. In the context of the vector wave equation, a number of preconditioning schemes have been proposed, where the operator is chosen to be the inverse of the vector wave operator. Efficient implementations of this type of preconditioner include multi-grid using low-order $\boldsymbol{H}(curl)$-conforming elements (Beck et al., 1999; Beck & Hiptmair, 1999; Gopalakrishnan et al., 2004), two-grid schemes for high-order $\boldsymbol{H}(curl)$-conforming elements (Pardo et al., 2006), and overlapping Schwarz-type methods (Gopalakrishnan & Pasciak, 2003). A key ingredient for multi-grid/two-grid approaches is an appropriate smoother for $\boldsymbol{H}(curl)$-conforming

[2]Despite conjugate gradients being unsuitable for the iterative solution of the unpreconditioned system in Eq. (3), they may still be used if the system is reformulated as a normal equation (e.g., Golub & Van Loan, 1996) or if the preconditioner is chosen in such a way that it takes care of the negative eigenvalues (Beck & Hiptmair, 1999).

elements; for further details, see Hiptmair (1998) and Arnold et al. (2000). Furthermore, an additional requirement for all these schemes is that the coarse grid is sufficiently fine in order to ensure convergence of the scheme.

The purpose of this work is to explore an alternative preconditioning strategy for the iterative solution of Eq. (3) when the *hp* finite elements of Schöberl and Zaglmayr (2005) are used. An operator-based preconditioner is employed that uses different operators for each part ($\mathcal{N}_0$, E, F, and I) of the discretization. The preconditioner takes advantage of the special construction of Zaglmayr and Schöberl's elements and has a block diagonal structure, which allows for an efficient and straightforward implementation. The work extends previous work by Zaglmayr (2006), which proposed a block diagonal preconditioner for the positive definite system matrix that is obtained in eddy current problems and regularized magnetostatic problems. It also builds on a previous study by Ledger (2009), which presented some initial two-dimensional numerical experiments for an indefinite preconditioner for Eq. (3). The presentation of material will proceed as follows: In Section 2, the construction of the preconditioner for indefinite problems and three-dimensional elements is described. Section 3 presents an analysis of the eigenspectrum of the system matrix as well as an investigation of the behavior of the eigenspectrum for the preconditioned system matrix. These investigations show that the performance of the preconditioner is dependent on the mesh spacing. The choice of the critical mesh spacing is addressed in Section 4. Numerical results, which illustrate the performance of the preconditioner for two- and three-dimensional problems, are presented in Section 5. The article ends with some concluding remarks.

2. Ingredients for the Preconditioner for Three-Dimensional Problems

In order to describe the iterative approach for solving Eq. (3), it is first beneficial to decompose K, x, and r into the blocks associated with the different types of basis functions the three-dimensional elements of Schöberl and Zaglmayr (2005):

$$K = \begin{pmatrix} K_{\mathcal{N}_0\mathcal{N}_0} & K_{\mathcal{N}_0 E} & K_{\mathcal{N}_0 F} & K_{\mathcal{N}_0 I} \\ K_{E\mathcal{N}_0} & K_{EE} & K_{EF} & K_{EI} \\ K_{F\mathcal{N}_0} & K_{FE} & K_{FF} & K_{FI} \\ K_{I\mathcal{N}_0} & K_{IE} & K_{IF} & K_{II} \end{pmatrix}, \qquad x = \begin{pmatrix} x_{\mathcal{N}_0} \\ x_E \\ x_F \\ x_I \end{pmatrix}, \qquad r = \begin{pmatrix} r_{\mathcal{N}_0} \\ r_E \\ r_F \\ r_I \end{pmatrix}. \quad (4)$$

If desired, one may also further decompose the face and interior blocks, as the basis functions associated with these blocks can themselves be split into those functions that are gradients of H^1 functions and those that are not. However, for conciseness of presentation, this additional decomposition is omitted. Note that K is itself made of a curl–curl part A and a mass part M, which is multiplied by κ, so that $K = A + \kappa M$, with A and M having the same block structure as K.

As p is increased, the number of interior degrees of freedom grows rapidly. In particular, for three-dimensional problems, they grow at the rate $O(p^3)$. The interior degrees of freedom are independent between each element, and consequently, a substantial reduction in the size of the linear system can be achieved by performing static condensation (e.g., Karniadakis & Sherwin, 1999). The condensed system corresponds to

$$\tilde{K}\tilde{x} = \tilde{r}, \quad (5)$$

where $\tilde{x} = (x_{\mathcal{N}_0} \;\; x_E \;\; x_F)^T$, and T denotes the vector transpose. Furthermore,

$$\tilde{K} = \begin{pmatrix} K_{\mathcal{N}_0\mathcal{N}_0} & K_{\mathcal{N}_0 E} & K_{\mathcal{N}_0 F} \\ K_{E\mathcal{N}_0} & K_{EE} & K_{EF} \\ K_{F\mathcal{N}_0} & K_{FE} & K_{FF} \end{pmatrix} - \begin{pmatrix} K_{\mathcal{N}_0 I} \\ K_{EI} \\ K_{FI} \end{pmatrix} K_{II}^{-1} (K_{I\mathcal{N}_0} \quad K_{IE} \quad K_{IF}), \tag{6}$$

$$\tilde{r} = \begin{pmatrix} r_{\mathcal{N}_0} \\ r_E \\ r_F \end{pmatrix} - \begin{pmatrix} K_{\mathcal{N}_0 I} \\ K_{EI} \\ K_{FI} \end{pmatrix} K_{II}^{-1} r_I. \tag{7}$$

Static condensation of the interior degrees of freedom is performed at the element level during the finite element assembly process. Note that the condensed matrix $\tilde{K}$ retains the same sparsity pattern as K and also inherits its indefinite property.

Based on previous experience (Ledger, 2009), the use of a modified version of Zaglmayr's preconditioner (Zaglmayr, 2006) is proposed for the iterative solution of $Kx = r$. The preconditioner takes the form C^{-1} with

$$C = \begin{pmatrix} K_{\mathcal{N}_0\mathcal{N}_0} & 0 & 0 & 0 \\ 0 & -\text{block diag}\,(|\kappa| M_{EE}) & 0 & 0 \\ 0 & 0 & \text{block diag}\,(A_{FF} + |\kappa| M_{FF}) & 0 \\ 0 & 0 & 0 & \text{block diag}\,(A_{II} + |\kappa| M_{II}) \end{pmatrix}. \tag{8}$$

Note that $A_{II} + |\kappa| M_{II}$ is block diagonal by construction, as the interior degrees of freedom are independent between elements. Also note that the curl–curl block for the higher-order edge functions is zero, and consequently, $-|\kappa| M_{EE} \equiv K_{EE}$. It has been expressed in this way because $|\kappa| M_{EE}$ is a positive definite matrix. If one chooses to additionally decompose the face and interior functions into gradients and nongradients, the blocks associated with face and interior functions that are gradients can then be treated in a similar way as the block for the higher-order edge functions in Eq. (8).

Similarly, the preconditioner $\tilde{C}^{-1}$ with

$$\tilde{C} = \begin{pmatrix} \tilde{K}_{\mathcal{N}_0\mathcal{N}_0} & 0 & 0 \\ 0 & -\text{block diag}\,(\tilde{B}_{EE}) & 0 \\ 0 & 0 & \text{block diag}\,(\tilde{B}_{FF}) \end{pmatrix} \tag{9}$$

is proposed for the iterative solution of $\tilde{K}\tilde{x} = \tilde{r}$. In the above, $B = A + |\kappa| M$ and $\tilde{B}$ follow from the static condensation of the interior block of B in the fictional linear system $By = 0$. The reason for following this approach is that the resulting blocks $\tilde{B}_{EE}$ and $\tilde{B}_{FF}$ are then positive definite (Ledger, 2009). If an additional decomposition of the face functions into gradients and nongradients is undertaken, the block associated with the gradient face functions can then be treated in similar way as the high order edge block in Eq. (9).

During the application of the iterative technique, it is necessary to repeatedly apply C^{-1} (or $\tilde{C}^{-1}$). Fortunately, due to the block diagonal structure of the preconditioner, its inverse can be computed block by block. For each block, the application of the inverse

to a known vector can be reformulated as a linear system. The lowest-order space plays a special role, and therefore, the application of $K^{-1}_{\mathcal{N}_0\mathcal{N}_0}$ (or $\tilde{K}^{-1}_{\mathcal{N}_0\mathcal{N}_0}$) is achieved by using a direct solver. The other blocks are positive definite; therefore, the application of the inverse of these blocks can be achieved approximately by using a standard iterative solver, such as conjugate gradients, or exactly by using a direct solver.

3. Analysis of the Eigenspectrum for Quadrilateral Elements

In Ledger (2009), numerical results were presented that showed that the eigenvalues of the preconditioned system became clustered about a point bounded away from zero once the mesh spacing was sufficiently small. In this section, a detailed investigation of the eigenspectrum of the preconditioners proposed in Eqs. (8) and (9) is undertaken for quadrilateral $\boldsymbol{H}(curl)$-conforming elements. Explicit bounds are obtained for the maximum and minimum eigenvalues of K and $\tilde{K}$ when the mesh consists of an infinite number of quadrilateral elements. The behavior of maximum and minimum values of $\mathrm{Re}(\lambda(C^{-1}K))$, and $\mathrm{Re}(\lambda(\tilde{C}^{-1}\tilde{K}))$ is also investigated. The complexity of this analytical calculation limits the analysis to second-order ($p = 1$) square $\boldsymbol{H}(curl)$-conforming elements. However, despite this limitation, the analysis does provide a valuable insight into how the choice of mesh spacing effects the eigenspectrum and, consequently, the performance of the preconditioner.

A typical square $\boldsymbol{H}(curl)$-conforming element is shown in Figure 1. Applying the approach of Schöberl and Zaglmayr (2005) to the construction of the basis functions on this element yields the lowest-order $p = 0$ edge basis functions

$$\boldsymbol{\phi}_1 = \begin{pmatrix} (n+1) - y/h \\ 0 \end{pmatrix}, \qquad \boldsymbol{\phi}_2 = \begin{pmatrix} y/h - n \\ 0 \end{pmatrix},$$

$$\boldsymbol{\phi}_3 = \begin{pmatrix} 0 \\ (m+1) - x/h \end{pmatrix}, \qquad \boldsymbol{\phi}_4 = \begin{pmatrix} 0 \\ x/h - m \end{pmatrix}.$$

These four functions make up the contributions to $V_{\mathcal{N}_0}$ for a single element. Continuing with Schöberl and Zaglmayr's approach, the higher-order edge basis functions for $p = 1$

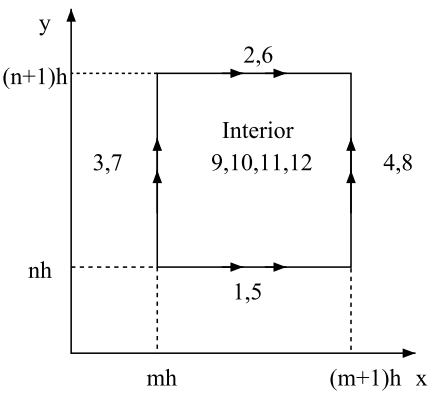

Figure 1. Square $\boldsymbol{H}(curl)$-conforming finite element.

on this square element are

$$\boldsymbol{\phi}_5 = \nabla\left[\left(\frac{1}{2}\left(\frac{2x}{h} - 2m - 1\right)^2 - \frac{1}{2}\right)\left(1 - \frac{y}{h} + n\right)\right],$$

$$\boldsymbol{\phi}_6 = \nabla\left[\left(\frac{1}{2}\left(\frac{2x}{h} - 2m - 1\right)^2 - \frac{1}{2}\right)\left(\frac{y}{h} - n\right)\right],$$

$$\boldsymbol{\phi}_7 = \nabla\left[\left(\frac{1}{2}\left(\frac{2y}{h} - 2n - 1\right)^2 - \frac{1}{2}\right)\left(1 - \frac{x}{h} + m\right)\right],$$

$$\boldsymbol{\phi}_8 = \nabla\left[\left(\frac{1}{2}\left(\frac{2y}{h} - 2n - 1\right)^2 - \frac{1}{2}\right)\left(\frac{x}{h} - m\right)\right],$$

and these basis functions make up the contributions to V_E for a single element. Finally, their four interior basis functions for this $p = 1$ square element are

$$\boldsymbol{\phi}_9 = \frac{1}{4}\nabla\left[\left(\left(\frac{y}{h} - n\right)^2 - 1\right)\left(\left(\frac{x}{h} - n\right)^2 - 1\right)\right],$$

$$\boldsymbol{\phi}_{10} = \frac{1}{4}\begin{pmatrix}\left(\left(\frac{y}{h} - n\right)^2 - 1\right)\frac{\mathrm{d}}{\mathrm{d}x}\left(\left(\frac{x}{h} - n\right)^2 - 1\right) \\ -\frac{\mathrm{d}}{\mathrm{d}y}\left(\left(\frac{y}{h} - n\right)^2 - 1\right)\left(\left(\frac{x}{h} - n\right)^2 - 1\right)\end{pmatrix},$$

$$\boldsymbol{\phi}_{11} = \frac{1}{2}\begin{pmatrix}\left(\left(\frac{y}{h} - n\right)^2 - 1\right) \\ 0\end{pmatrix},$$

$$\boldsymbol{\phi}_{12} = \frac{1}{2}\begin{pmatrix}0 \\ \left(\left(\frac{x}{h} - m\right)^2 - 1\right)\end{pmatrix}.$$

These four functions make up the contributions to V_I for this element. A $p = 1$ approximation of the electric field over this element is then given by the sum

$$\boldsymbol{E}_H = \sum_{n=1}^{12} \alpha_n \boldsymbol{\phi}_n, \tag{10}$$

where α_n are the degrees of freedom that are associated with weighted tangential moments of the electric field.

Strang and Fix (1973) outlined a procedure for computing upper and lower bounds for the eigenvalues of finite element system matrices for meshes of bi-linear quadrilateral elements. A similar procedure is followed in this work, except that $\boldsymbol{H}(curl)$-conforming rather than H^1-conforming finite elements are used. The use of these more exotic finite elements complicates the procedure. Fortunately, however, the initial stages of the approach used for determining the bounds on the eigenvalues of the system matrices

follows that used by Ainsworth and Coyle (2001) to investigate the dispersive behavior of $p = 0$ square $\boldsymbol{H}(curl)$-conforming finite elements. Following the analysis of Ainsworth and Coyle, an infinite mesh of square elements is considered on which unit values for ϵ and μ are assumed. Three typical elements X, Y, and Z, which are shown in Figure 2, are required for analysis. On these elements, those weighting functions associated with the two edges indicated in bold (one horizontal and one vertical), as well as those associated with the interiors of the elements, need to be considered. However, rather than just using the $p = 0$ basis functions used in the dispersion analysis presented in Ainsworth and Coyle (2001), the complete set of basis functions for a $p = 1$ approximation are considered. An investigation for the $p = 0$ approximation would not be worthwhile for the proposed preconditioner. The $p = 1$ basis functions for element X are identical to those already presented. The basis functions for elements Y and Z can be developed in a similar manner. The choice of $\boldsymbol{w} = \boldsymbol{\phi}_1$ in Equation (2) yields

$$
\begin{aligned}
k(\boldsymbol{E}, \boldsymbol{\phi}_1)_\Omega = {} & k(\boldsymbol{\phi}_1, \boldsymbol{\phi}_1)_{X\cup Z}\alpha_1 + k(\boldsymbol{\phi}_2, \boldsymbol{\phi}_1)_X\alpha_2 + k(\boldsymbol{\phi}_3, \boldsymbol{\phi}_1)_{X\cup Y}\alpha_3 + k(\boldsymbol{\phi}_4, \boldsymbol{\phi}_1)_X\alpha_4 \\
& + k(\boldsymbol{\phi}_5, \boldsymbol{\phi}_1)_{X\cup Z}\alpha_5 + k(\boldsymbol{\phi}_6, \boldsymbol{\phi}_1)_X\alpha_6 + k(\boldsymbol{\phi}_7, \boldsymbol{\phi}_1)_{X\cup Y}\alpha_7 + k(\boldsymbol{\phi}_8, \boldsymbol{\phi}_1)_X\alpha_8 \\
& + k(\boldsymbol{\phi}_9, \boldsymbol{\phi}_1)_X\alpha_9 + k(\boldsymbol{\phi}_{10}, \boldsymbol{\phi}_1)_X\alpha_{10} + k(\boldsymbol{\phi}_{11}, \boldsymbol{\phi}_1)_X\alpha_{11} + k(\boldsymbol{\phi}_{12}, \boldsymbol{\phi}_1)_X\alpha_{12} \\
& + k(\boldsymbol{\phi}_{13}, \boldsymbol{\phi}_1)_Z\alpha_{13} + k(\boldsymbol{\phi}_{14}, \boldsymbol{\phi}_1)_Z\alpha_{14} + k(\boldsymbol{\phi}_{15}, \boldsymbol{\phi}_1)_Z\alpha_{15} + k(\boldsymbol{\phi}_{16}, \boldsymbol{\phi}_1)_Z\alpha_{16} \\
& + k(\boldsymbol{\phi}_{17}, \boldsymbol{\phi}_1)_Z\alpha_{17} + k(\boldsymbol{\phi}_{18}, \boldsymbol{\phi}_1)_Z\alpha_{18} + k(\boldsymbol{\phi}_{19}, \boldsymbol{\phi}_1)_Z\alpha_{19} + k(\boldsymbol{\phi}_{20}, \boldsymbol{\phi}_1)_Z\alpha_{20} \\
& + k(\boldsymbol{\phi}_{21}, \boldsymbol{\phi}_1)_Z\alpha_{21} + k(\boldsymbol{\phi}_{22}, \boldsymbol{\phi}_1)_Z\alpha_{22} + k(\boldsymbol{\phi}_{23}, \boldsymbol{\phi}_1)_Y\alpha_{23} + k(\boldsymbol{\phi}_{24}, \boldsymbol{\phi}_1)_Y\alpha_{24} \\
& + k(\boldsymbol{\phi}_{25}, \boldsymbol{\phi}_1)_Y\alpha_{25} + k(\boldsymbol{\phi}_{26}, \boldsymbol{\phi}_1)_Y\alpha_{26} + k(\boldsymbol{\phi}_{27}, \boldsymbol{\phi}_1)_Y\alpha_{27} + k(\boldsymbol{\phi}_{28}, \boldsymbol{\phi}_1)_Y\alpha_{28} \\
& + k(\boldsymbol{\phi}_{29}, \boldsymbol{\phi}_1)_Y\alpha_{29} + k(\boldsymbol{\phi}_{30}, \boldsymbol{\phi}_1)_Y\alpha_{30} + k(\boldsymbol{\phi}_{31}, \boldsymbol{\phi}_1)_Y\alpha_{31} + k(\boldsymbol{\phi}_{32}, \boldsymbol{\phi}_1)_Y\alpha_{32}.
\end{aligned}
$$

Similar expressions can be found for the choices $\boldsymbol{w} = \boldsymbol{\phi}_3$, $\boldsymbol{w} = \boldsymbol{\phi}_5$, and $\boldsymbol{w} = \boldsymbol{\phi}_7$. In addition, expressions can also be obtained for $k(\boldsymbol{E}, \boldsymbol{w})_\Omega$ for the weighting functions

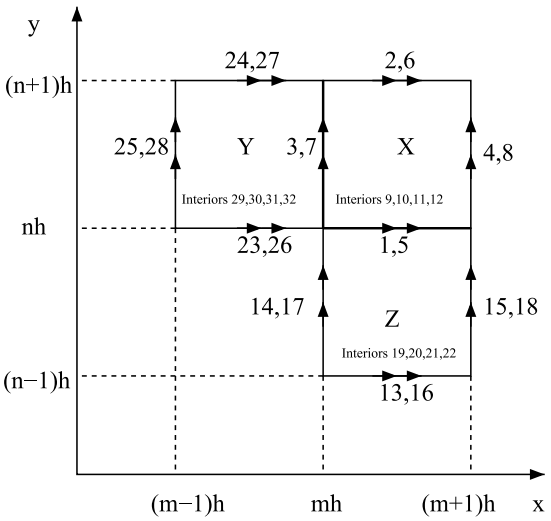

Figure 2. Three typical square elements in an infinite mesh.

associated with the interior degrees of freedom in elements X, Y, and Z. Just as in the dispersion analysis of Ainsworth and Coyle (2001), the finite element solution is assumed to be an interpolated plane wave:

$$\boldsymbol{E}_H = \boldsymbol{E}_0\{\mathrm{i}(\xi_x x + \xi_y y)\},$$

where $\mathrm{i} = \sqrt{-1}$. For this choice, it follows that by fixing the coefficients α_1, α_3, α_5, and α_7, the coefficients associated with the other edges of elements X, Y, and Z can be written in terms of these values as follows:

$$\begin{aligned}
\alpha_2 &= \mathrm{i}\xi_y h\alpha_1, & \alpha_4 &= \mathrm{i}\xi_x h\alpha_3,\\
\alpha_6 &= \mathrm{i}\xi_y h\alpha_5, & \alpha_8 &= \mathrm{i}\xi_x h\alpha_7,\\
\alpha_{13} &= -\mathrm{i}\xi_y h\alpha_1, & \alpha_{14} &= -\mathrm{i}\xi_y h\alpha_3,\\
\alpha_{15} &= \mathrm{i}(\xi_x h - \xi_y h)\alpha_3, & \alpha_{16} &= -\mathrm{i}\xi_y h\alpha_5,\\
\alpha_{17} &= -\mathrm{i}\xi_y h\alpha_7, & \alpha_{18} &= \mathrm{i}(\xi_x h - \xi_y h)\alpha_7,\\
\alpha_{23} &= -\mathrm{i}\xi_x h\alpha_1, & \alpha_{24} &= \mathrm{i}(\xi_y h - \xi_x h)\alpha_1,\\
\alpha_{25} &= -\mathrm{i}\xi_x h\alpha_3, & \alpha_{26} &= -\mathrm{i}\xi_x h\alpha_5,\\
\alpha_{27} &= \mathrm{i}(\xi_y h - \xi_x h)\alpha_5, & \alpha_{28} &= -\mathrm{i}\xi_x h\alpha_7.
\end{aligned}$$

Note, however, that the coefficients associated with the interiors of the elements remain independent and, hence, uncoupled. The introduction of this simplification allows the problem to be reduced to the *small* linear system $K^S\alpha = 0$ with entries

$$\begin{pmatrix} k^S_{11} & k^S_{13} & k^S_{15} & k^S_{17} & k^S_{1I}\\ k^S_{31} & k^S_{33} & k^S_{35} & k^S_{37} & k^S_{3I}\\ k^S_{51} & k^S_{53} & k^S_{55} & k^S_{57} & k^S_{5I}\\ k^S_{71} & k^S_{73} & k^S_{75} & k^S_{77} & k^S_{7I}\\ k^S_{I1} & k^S_{I3} & k^S_{I5} & k^S_{I7} & k^S_{II} \end{pmatrix} \begin{pmatrix} \alpha_1\\ \alpha_3\\ \alpha_5\\ \alpha_7\\ \alpha_I \end{pmatrix} = \begin{pmatrix} 0\\ 0\\ 0\\ 0\\ 0 \end{pmatrix}, \tag{11}$$

or in block form

$$\begin{pmatrix} K^S_{\mathcal{N}_0\mathcal{N}_0} & K^S_{\mathcal{N}_0 E} & K^S_{\mathcal{N}_0 I}\\ K^S_{E\mathcal{N}_0} & K^S_{EE} & K^S_{EI}\\ K^S_{I\mathcal{N}_0} & K^S_{IE} & K^S_{II} \end{pmatrix} \begin{pmatrix} \alpha_{\mathcal{N}_0}\\ \alpha_E\\ \alpha_I \end{pmatrix} = 0.$$

In the above, the symbol I has been used to represent the 12 degrees of freedom associated with the interior of the three elements X, Y, and Z. This linear system has a very similar block structure to that of $Kx = r$, except that there are no face blocks as this is a two-dimensional problem. In Eq. (11) the coefficients α_1 and α_3 are the lowest order, $p = 0$, edge degrees of freedom associated with edges 1 and 3, and the coefficients α_5 and α_7 are the higher order, $p = 1$, edge degrees of freedom associated with the same two edges. Despite the matrix K^S having a similar block structure to K, it has complex rather than real entries because of the assumption made about the form of the solution.

It has, however, reduced a problem set on an infinite mesh of elements to a linear system of finite dimension.

The entries in K^S are readily computable using a symbolic mathematics package such as MAPLE, MATHEMATICA, or the symbolic toolbox in MATLAB (The Mathworks, Natick, Massachusetts, USA). In this work, the latter of these packages is used to evaluate the entries associated with various blocks. For example, the entries associated with the $K^S_{\mathcal{N}_0\mathcal{N}_0}$ block are

$$k^S_{11} = \frac{2}{h^2}(1-\cos\theta) - \frac{\omega^2}{3}(2+\cos\theta),$$

$$k^S_{13} = \frac{1}{h^2}(-1+\exp(\mathrm{i}\psi)+\exp(-\mathrm{i}\theta)-\exp(\mathrm{i}(\psi-\theta))) = (k^S_{31})^*,$$

$$k^S_{33} = \frac{2}{h^2}(1-\cos\psi) - \frac{\omega^2}{3}(2+\cos\psi),$$

where $\theta = h\xi_y$, $\psi = h\xi_x$, and $*$ denotes the complex conjugate. Similar, albeit longer, expressions can be found for the other entries of K^S. Clearly, θ and ψ can be interpreted as angles measured in radians with values in the range $0 \leq \theta,\ \psi \leq 2\pi$. To investigate the eigenspectrum of K, the eigenvalue problem $K^s\alpha = \lambda\alpha$ with entries

$$\begin{pmatrix} k^S_{11} & k^S_{13} & k^S_{15} & k^S_{17} & k^S_{1I} \\ k^S_{31} & k^S_{33} & k^S_{35} & k^S_{37} & k^S_{3I} \\ k^S_{51} & k^S_{53} & k^S_{55} & k^S_{57} & k^S_{5I} \\ k^S_{71} & k^S_{73} & k^S_{75} & k^S_{77} & k^S_{7I} \\ k^S_{I1} & k^S_{I3} & k^S_{I5} & k^S_{I7} & k^S_{II} \end{pmatrix} \begin{pmatrix} \alpha_1 \\ \alpha_3 \\ \alpha_5 \\ \alpha_7 \\ \alpha_I \end{pmatrix} = \lambda \begin{pmatrix} \alpha_1 \\ \alpha_3 \\ \alpha_5 \\ \alpha_7 \\ \alpha_I \end{pmatrix}, \tag{12}$$

will be considered. On the other hand, if the interior degrees of freedom are eliminated from Eq. (11) using static condensation, the linear system $\tilde{K}^S\tilde{\alpha} = 0$ is obtained. To examine the eigenspectrum of $\tilde{K}$, the smaller eigenvalue problem $\tilde{K}^S\tilde{\alpha} = \lambda\tilde{\alpha}$ with entries

$$\begin{pmatrix} \tilde{k}^S_{11} & \tilde{k}^S_{13} & \tilde{k}^S_{15} & \tilde{k}^S_{17} \\ \tilde{k}^S_{31} & \tilde{k}^S_{33} & \tilde{k}^S_{35} & \tilde{k}^S_{37} \\ \tilde{k}^S_{51} & \tilde{k}^S_{53} & \tilde{k}^S_{55} & \tilde{k}^S_{57} \\ \tilde{k}^S_{71} & \tilde{k}^S_{73} & \tilde{k}^S_{75} & \tilde{k}^S_{77} \end{pmatrix} \begin{pmatrix} \alpha_1 \\ \alpha_3 \\ \alpha_5 \\ \alpha_7 \end{pmatrix} = \lambda \begin{pmatrix} \alpha_1 \\ \alpha_3 \\ \alpha_5 \\ \alpha_7 \end{pmatrix}, \tag{13}$$

will be considered. By considering the eigenvalues of $K^S\alpha = \lambda C^S\alpha$ with entries

$$\begin{pmatrix} k^S_{11} & k^S_{13} & k^S_{15} & k^S_{17} & k^S_{1I} \\ k^S_{31} & k^S_{33} & k^S_{35} & k^S_{37} & k^S_{3I} \\ k^S_{51} & k^S_{53} & k^S_{55} & k^S_{57} & k^S_{5I} \\ k^S_{71} & k^S_{73} & k^S_{75} & k^S_{77} & k^S_{7I} \\ k^S_{I1} & k^S_{I3} & k^S_{I5} & k^S_{I7} & k^S_{II} \end{pmatrix} \begin{pmatrix} \alpha_1 \\ \alpha_3 \\ \alpha_5 \\ \alpha_7 \\ \alpha_I \end{pmatrix} = \lambda \begin{pmatrix} k^S_{11} & k^S_{13} & 0 & 0 & 0 \\ k^S_{31} & k^S_{33} & 0 & 0 & 0 \\ 0 & 0 & -b^S_{55} & 0 & 0 \\ 0 & 0 & 0 & -b^S_{77} & 0 \\ 0 & 0 & 0 & 0 & b^S_I \end{pmatrix} \begin{pmatrix} \alpha_1 \\ \alpha_3 \\ \alpha_5 \\ \alpha_7 \\ \alpha_I \end{pmatrix}, \tag{14}$$

the eigenspectrum of $C^{-1}K$ will be investigated. In the above expression, the entries b^S_{55}, b^S_{77}, and b^S_I are determined in a similar way to the entries in K^S, except that they arise

from considering the edge element discretization of the fictional weak variational statement $(curl\boldsymbol{E}, curl\boldsymbol{W}) + (|\kappa|\boldsymbol{E}, \boldsymbol{W}) = 0$. Considering the same infinite mesh of squares and forcing the solution to be the same plane wave, one may obtain the linear system $B^S\alpha = 0$, of which b^S_{55}, b^S_{77}, and b^S_I are particular entries. Finally by considering the eigenvalues of $\tilde{K}^S\tilde{\alpha} = \lambda\tilde{C}^S\tilde{\alpha}$ with entries

$$\begin{pmatrix} \tilde{k}^S_{11} & \tilde{k}^S_{13} & \tilde{k}^S_{15} & \tilde{k}^S_{17} \\ \tilde{k}^S_{31} & \tilde{k}^S_{33} & \tilde{k}^S_{35} & \tilde{k}^S_{37} \\ \tilde{k}^S_{51} & \tilde{k}^S_{53} & \tilde{k}^S_{55} & \tilde{k}^S_{57} \\ \tilde{k}^S_{71} & \tilde{k}^S_{73} & \tilde{k}^S_{75} & \tilde{k}^S_{77} \end{pmatrix} \begin{pmatrix} \alpha_1 \\ \alpha_3 \\ \alpha_5 \\ \alpha_7 \end{pmatrix} = \lambda \begin{pmatrix} \tilde{k}^S_{11} & \tilde{k}^S_{13} & 0 & 0 \\ \tilde{k}^S_{31} & \tilde{k}^S_{33} & 0 & 0 \\ 0 & 0 & -\tilde{b}^S_{55} & 0 \\ 0 & 0 & 0 & -\tilde{b}^S_{77} \end{pmatrix} \begin{pmatrix} \alpha_1 \\ \alpha_3 \\ \alpha_5 \\ \alpha_7 \end{pmatrix}, \tag{15}$$

the eigenspectrum of $\tilde{C}^{-1}\tilde{K}$ will be investigated. In the above, $\tilde{b}^S_{55}$ and $\tilde{b}^S_{77}$ result from performing static condensation on $B^S\alpha = 0$, resulting in the elimination of the interior block in B^S. Investigating the eigenvalues of this system will allow the eigenspectrum of $\tilde{C}^{-1}\tilde{K}$ to be investigated.

3.1. Eigenspectrum of K

Recall that K is a real symmetric indefinite matrix with positive and negative real eigenvalues. To construct bounds on the eigenvalues of K, the matrix K^S is used. The matrix K^S is Hermitian, and consequently, all of its eigenvalues are real (Strang, 1976). Naturally, the eigenvalues of K^S will be a function of the angles θ and ψ, as well as h and ω. The maximum and minimum eigenvalues for any given combination of h and ω will occur at situations where $\lambda(K^S)$ is maximized or minimized over the range of angles $0 \leq \theta, \psi \leq 2\pi$.

By examining different combinations of θ and ψ, it can be found that the maximum eigenvalue occurs when $\theta = \psi = \pi$ and takes the form

$$\lambda_{\max}(K^S) = -\frac{1}{3}\left(\omega^2 - \frac{24}{h^2}\right). \tag{16}$$

The minimum eigenvalue occurs when $\theta = \pi$, $\psi = 0$ or when $\theta = 0$, $\psi = \pi$. For conciseness of presentation, the expression for the minimum eigenvalue is presented in the form of a truncated Taylor series:

$$\lambda_{\min}(K^S) = -\frac{89}{90}\omega^2 - \frac{1}{90}\omega^2\sqrt{3{,}601} - \frac{41}{600}\omega^4h^2 - \frac{803}{720{,}200}\omega^4h^2\sqrt{3{,}601} + O(\omega^6h^4), \tag{17}$$

which, for small h, becomes

$$\lambda_{\min}(K^S) \approx -\frac{89}{90}\omega^2 - \frac{1}{90}\omega^2\sqrt{3{,}601}. \tag{18}$$

As the maximum and minimum eigenvalues of K^S bound those of K (Strang & Fix, 1973),

$$-\frac{89}{90}\omega^2 - \frac{1}{90}\omega^2\sqrt{3{,}601} - \frac{41}{600}\omega^4h^2 - \frac{803}{720{,}200}\omega^4h^2\sqrt{3{,}601} + O(\omega^6h^4)$$
$$\leq \lambda(K) \leq -\frac{1}{3}\left(\omega^2 - \frac{24}{h^2}\right). \tag{19}$$

The behavior of the smallest and largest eigenvalues of K^S with varying mesh spacing for $\omega^2 = 1{,}000$ is shown in Figure 3. In this figure, it is clearly observable that as the mesh is refined, the gap between smallest and largest eigenvalue widens. This behavior has important implications for the performance of iterative solution techniques applied to $Kx = r$. First recall that for symmetric positive definite matrices, the number of iterations required by conjugate gradients to reduce the residual to a specified tolerance depends not only on the dimensions of the matrix but also on its condition number (Saad, 1996). The condition number for such matrices is given by

$$\chi = \left| \frac{\lambda_{\max}}{\lambda_{\min}} \right|. \tag{20}$$

Ainsworth and Coyle (2003a) presented bounds on this quantity for the system mass and curl–curl matrices that are obtained when $\kappa > 0$ and when discretizations consisting of *hp* quadrilateral/hexahedral $\boldsymbol{H}(curl)$-conforming finite elements are used.

However, for general indefinite matrices, the number of iterations required by iterative techniques, such as QMR, GMRES, or BICG, depends not only on the size of the matrix but also on how the eigenvalues are spread out across the complex plane. The closer that the eigenvalues are clustered about a point bounded away from zero, the faster the convergence of the iterative technique (Saad, 1996). The bounds on the eigenvalues of K indicates that the gap between the largest and smallest eigenvalues will widen rapidly as the mesh is refined. Consequently, this means that the number of iterations will grow quickly and the performance of the iterative technique will deteriorate as the mesh is refined. This is not good news, as mesh refinement is, of course, needed to improve

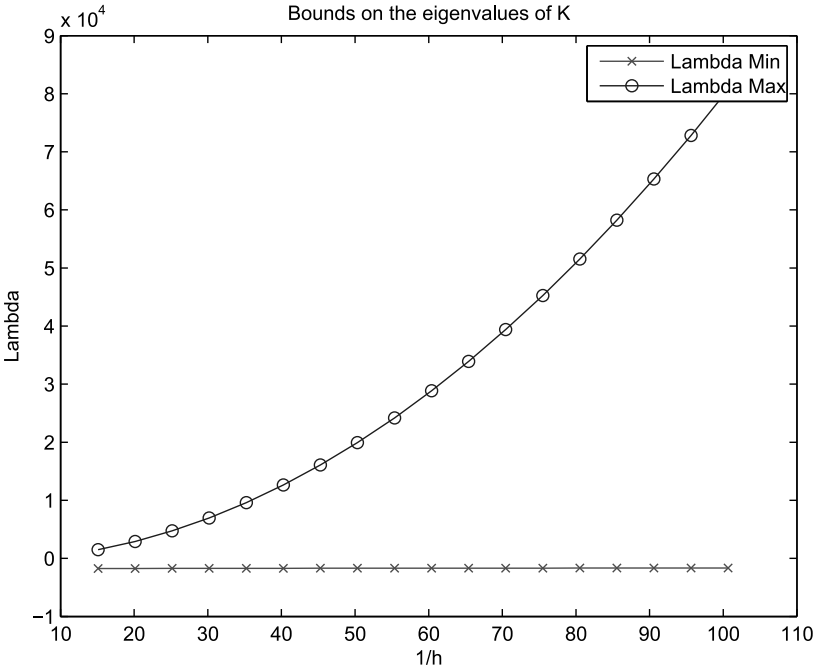

Figure 3. Behavior of $\lambda_{\max}(K^S)$ and $\lambda_{\min}(K^S)$ with h refinement.

the accuracy of the finite element solution. Thus, without a suitable preconditioner, the application of an iterative solver to $Kx = r$ is doomed to failure.

3.2. *Eigenspectrum of $\tilde{K}$*

The matrix $\tilde{K}$ is obtained by performing static condensation on K; the matrix $\tilde{K}$ is also the Schur complement of K. Like K, $\tilde{K}$ is symmetric and indefinite and, consequently, has positive and negative real eigenvalues. To construct bounds on the eigenvalues of $\tilde{K}$, the matrix $\tilde{K}^S$ is considered. The matrix $\tilde{K}^S$ is the Schur complement of K^S. The inverse of an invertible Hermitian matrix is also Hermitian, and therefore, it also follows that its Schur complement will also be a Hermitian matrix and have real eigenvalues. The eigenvalues themselves will be a function of the angles θ and ψ, as well as h and ω. The maximum and minimum eigenvalues for any given combination of h and ω correspond to situations where $\lambda(\tilde{K}^S)$ is maximized or minimized over the range of angles $0 \leq \theta, \psi \leq 2\pi$. By examining different combinations of θ and ψ, it can be found that the maximum eigenvalue occurs when $\theta = \psi = \pi$ and has the value

$$\lambda_{\max}(\tilde{K}^S) = -\frac{1}{3}\left(\omega^2 - \frac{24}{h^2}\right). \tag{21}$$

The minimum eigenvalue occurs when $\theta = \pi$, $\psi = 0$ or when $\theta = 0$, $\psi = \pi$ and can be explicitly obtained for the case when $h < \Lambda$ (where $\omega = 2\pi/\Lambda$) as

$$\lambda_{\min}(\tilde{K}^S) = -\frac{1}{36}\frac{(11\omega^2h^2 - 356 - 25(\omega^4h^4 + 40\omega^2h^2 + 57616)^{1/2})\omega^2}{\omega^2h^2 - 10}. \tag{22}$$

Therefore, following bounds on the eigenvalues of $\tilde{K}$ for $h < \Lambda$ are

$$-\frac{1}{36}\frac{(11\omega^2h^2 - 356 - 25(\omega^4h^4 + 40\omega^2h^2 + 57616)^{1/2})\omega^2}{\omega^2h^2 - 10} \leq \lambda(\tilde{K}) \leq -\frac{1}{3}\left(\omega^2 - \frac{24}{h^2}\right). \tag{23}$$

The behavior of the smallest and largest eigenvalues with varying mesh spacing for the particular case of $\omega^2 = 1{,}000$ is shown in Figure 4. As in the case without static condensation, it is observed that as the mesh is refined, the gap between smallest and largest eigenvalue widens. This means that the performance of iterative solution techniques is expected to deteriorate for small h. Comparing the maximum and minimum eigenvalues of K^S and $\tilde{K}^S$, it is found that $\lambda_{\max}(\tilde{K}^S) = \lambda_{\max}(K^S)$ and $\lambda_{\min}(\tilde{K}^S) \approx \lambda_{\min}(K^S)$ for small h. Despite the fact that similar bounds have been obtained for both $\lambda(K)$ and $\lambda(\tilde{K})$, it is expected that an iterative solution technique will perform slightly better for $\tilde{K}$ than K because of the reduction in the size of the linear system that occurs when static condensation is performed.

3.3. *Eigenspectrum of $C^{-1}K$*

The preconditioning matrix C is real, symmetric, and indefinite. When it is applied to K, which is also real, symmetric, and indefinite, the resulting matrix $C^{-1}K$ is no longer symmetric, and consequently, its eigenvalues will be complex. To study the eigenspectrum

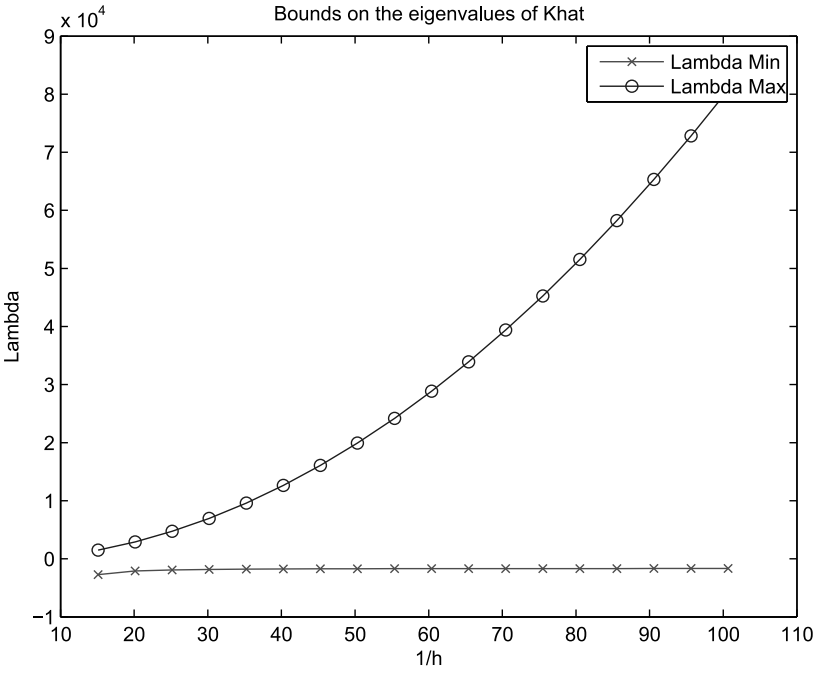

Figure 4. Behavior of $\lambda_{\max}(\tilde{K}^S)$ and $\lambda_{\min}(\tilde{K}^S)$ with h refinement.

of the matrix $C^{-1}K$, the eigenvalues of the matrix $(C^S)^{-1}K^S$ are investigated. The matrices C^S and K^S are both Hermitian; however, as $(C^S)^{-1}K^S \neq K^S(C^S)^{-1}$, the matrix $(C^S)^{-1}K^S$ cannot be Hermitian, and consequently, its eigenvalues will be complex.

Unfortunately, it is not possible to get explicit bounds for either the real or imaginary parts of the eigenvalues of $(C^S)^{-1}K^S$. In the previous cases, the maximum and minimum eigenvalues were found by maximizing or minimizing λ, a task that was made easier, as the maximum and minimum eigenvalues corresponded to where $\cos\theta = \pm 1$ and $\cos\psi = \pm 1$. However, $\lambda((C^S)^{-1}K^S)$ is a complicated nonlinear function of trigonometric functions of the angles θ and ψ, and consequently, the maximum and minimum real and imaginary parts of the eigenvalues will not only vary with h but also with θ and ψ. Nevertheless, by studying the eigenspectrum at a set of discrete values of θ and ψ ($\theta_i, \psi_i = i\pi/16, i = 0, 1, \ldots, 31$), and then varying h, it can be found that the maximum and minimum real parts of $\lambda((C^S)^{-1}K^S)$ have the following behavior:

$$\min(\mathrm{Re}(\lambda((C^S)^{-1}K^S))) \nearrow -1 - \frac{\sqrt{30}}{6}, \qquad \max(\mathrm{Re}(\lambda((C^S)^{-1}K^S))) \searrow 1,$$

as $h \to 0$. As the eigenvalues of $(C^S)^{-1}K^S$ bound those of $C^{-1}K$, it is expected that for sufficiently fine h,

$$-1 - \frac{\sqrt{30}}{6} \leq \mathrm{Re}(\lambda((C)^{-1}K)) \leq 1. \tag{24}$$

The behavior of the eigenfunctions corresponding to the combinations of θ_i and ψ_i, which give rise to the maximum and minimum values of $\mathrm{Re}(\lambda((C^S)^{-1}K^S))$ at a particular value of h, for $\omega^2 = 1{,}000$ are shown in Figure 5. The different line types in this figure indicate

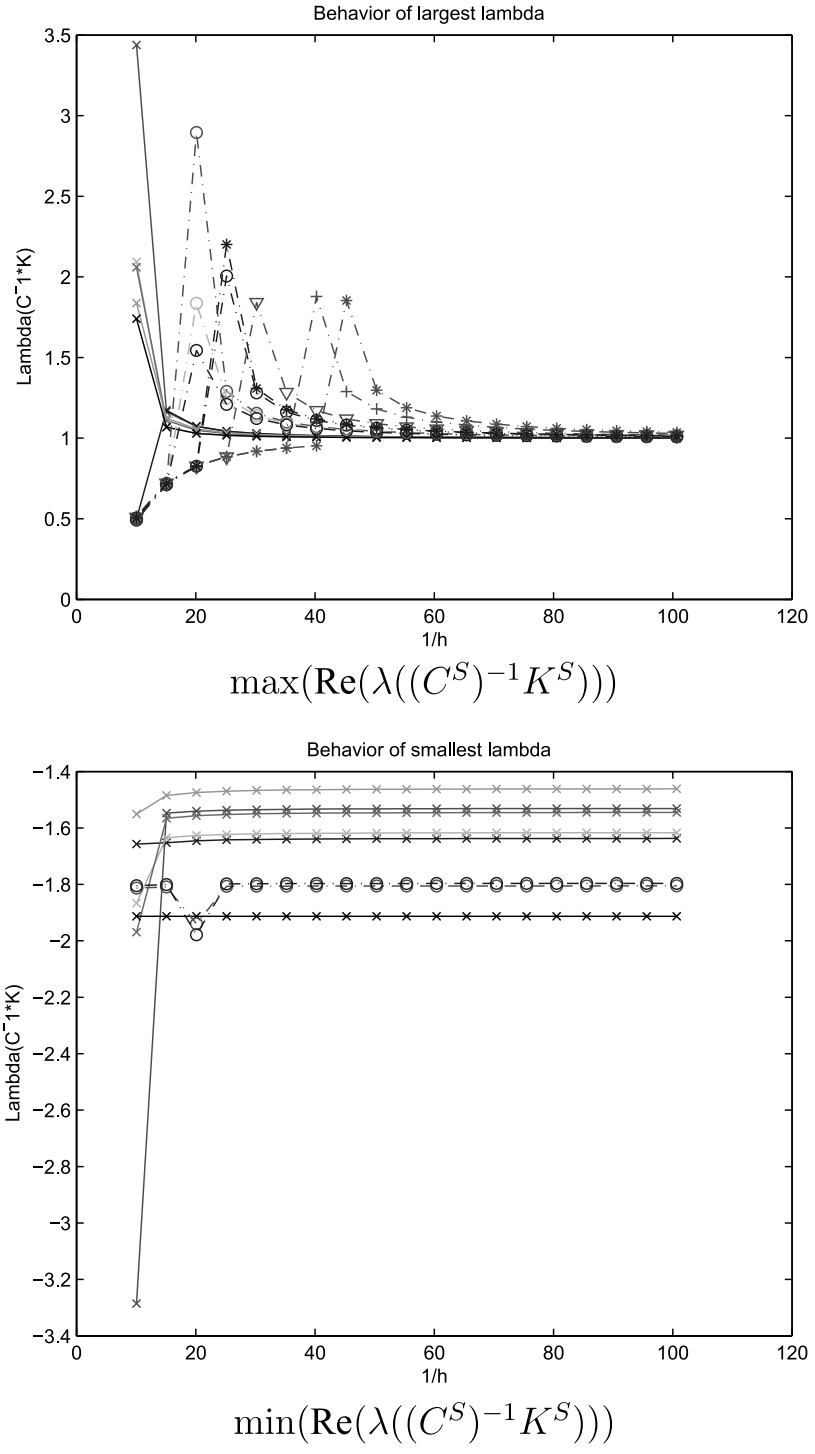

Figure 5. Behavior of $\max(\mathrm{Re}(\lambda((C^S)^{-1}K^S)))$ and $\min(\mathrm{Re}(\lambda((C^S)^{-1}K^S)))$ at discrete values of θ and ψ with h refinement.

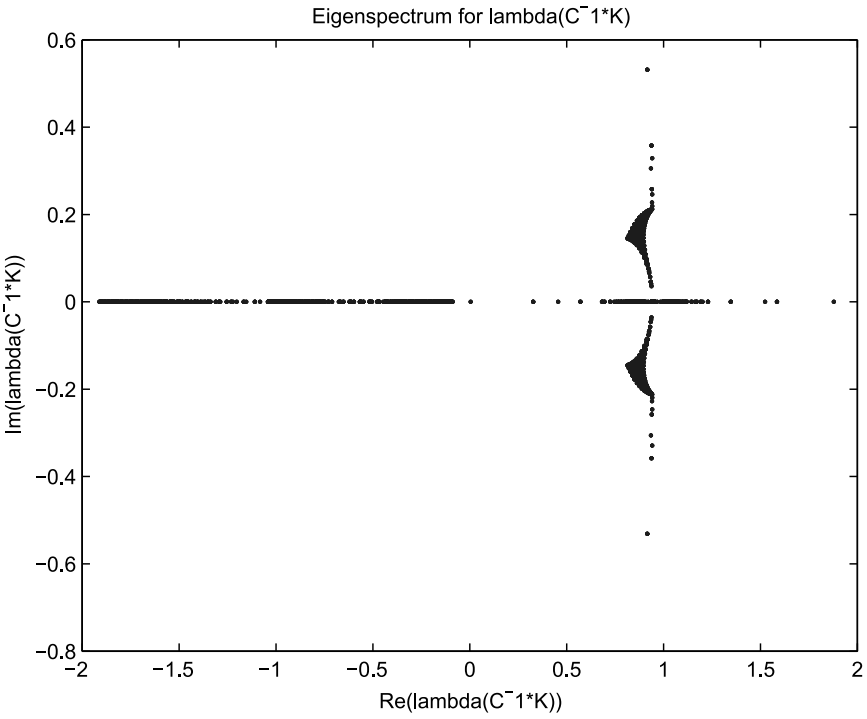

Figure 6. Eigenspectrum of $\lambda((C^S)^{-1}K^S)$ for discrete values of θ and ψ.

the eigenfunctions associated with different discrete values of θ and ψ. One can observe how different eigenfunctions give rise to maxima and minima for $\mathrm{Re}(\lambda((C^S)^{-1}K^S))$, as h is varied. Indeed, as h is reduced, the trend stated earlier for sufficiently small h can also be observed.

This study indicates the benefits that the preconditioner can bring for the system without static condensation. Rather than an eigenspectrum that grows with ω and h, the real part of the eigenspectrum falls within specified upper and lower bounds, once h is chosen to be sufficiently small. In particular, as h is refined, the maximum and minimum values of $\mathrm{Re}(\lambda((C^S)^{-1}K^S))$ will approach 1 and $-1-\sqrt{30}/6$, respectively. A typical plot of the eigenspectrum of $(C^S)^{-1}K^S$ for $\omega^2 = 1{,}000$ and $h = \Lambda/8$ is shown in Figure 6. This figure indicates the distribution of the eigenvalues in the complex plane and the way in which they surround a point that is bounded away from zero. The pattern in which the eigenvalues cluster is precisely what is required in order for iterative solvers, such as QMR, GMRES, and BICG, to converge. The fact that the real parts of the eigenvalues become bounded from above and below, once the mesh is sufficiently fine, indicates that the preconditioner will perform in a robust manner with h refinement.

3.4. Eigenspectrum of $\tilde{C}^{-1}\tilde{K}$

The preconditioning matrix $\tilde{C}$ is real, symmetric, and indefinite. When it is applied to $\tilde{K}$, which is also real, symmetric, and indefinite, the resulting matrix $\tilde{C}^{-1}\tilde{K}$ is no longer symmetric, and consequently, its eigenvalues will be complex. To study the eigenspectrum of this matrix, the eigenvalues of the matrix $(\tilde{C}^S)^{-1}\tilde{K}^S$ are investigated. The matrices

$\tilde{C}^S$ and $\tilde{K}^S$ are both Hermitian, but $(\tilde{C}^S)^{-1}\tilde{K}^S$ is not, and consequently, its eigenvalues are complex.

No explicit bounds can be found for the eigenvalues of $(\tilde{C}^S)^{-1}\tilde{K}^S$ due to their dependence on θ and ψ. However, by studying the eigenvalues of $(\tilde{C}^S)^{-1}\tilde{K}^S$ at the same discrete values of θ and ψ that were considered in Section 3.3, one can observe the trend

$$\min(\mathrm{Re}(\lambda((\tilde{C}^S)^{-1}\tilde{K}^S))) \nearrow \frac{2}{7}, \qquad \max(\mathrm{Re}(\lambda((\tilde{C}^S)^{-1}\tilde{K}^S))) \searrow 1 + \frac{\sqrt{55}}{11},$$

as $h \to 0$. This indicates that for sufficiently small h,

$$\frac{2}{7} \leq \mathrm{Re}(\lambda((\tilde{C})^{-1}\tilde{K})) \leq 1 + \frac{\sqrt{55}}{11} \tag{25}$$

is expected. Comparing this with the previous results for the preconditioner without static condensation indicates that the clustering of the eigenvalues is tighter in the limit as $h \to 0$ with static condensation than without. The behavior of the smallest and largest values of $\mathrm{Re}(\lambda((\tilde{C}^S)^{-1}\tilde{K}^S))$ with varying mesh spacing for $\omega^2 = 1{,}000$ is shown in Figure 7. The different line types used in this figure indicate the eigenfunctions associated with different discrete values of θ and ψ. One can observe how different eigenfunctions give rise to maxima and minima for $\mathrm{Re}(\lambda((C^S)^{-1}K^S))$ as h is varied. Indeed, as h is reduced, the trend stated earlier for sufficiently small h can also be observed.

As in the case of the preconditioned system without static condensation, it can be observed that the real part of the eigenspectrum falls within upper and lower bounds, once h is sufficiently small. It is therefore expected that the preconditioner will perform in a robust manner with mesh refinement. Moreover, as the bounds are tighter than those for preconditioning without static condensation, iterative solvers are expected to perform much better in this case. A typical plot of the eigenspectrum for $(\tilde{C}^S)^{-1}\tilde{K}^S$ for $\omega^2 = 1{,}000$ and $h = \Lambda/8$ is shown in Figure 8. This figure closely resembles the numerical results presented previously in Ledger (2009) for actual eigenspectra of preconditioned system matrices for meshes of $p = 1$ quadrilateral elements. As in Ledger (2009), the eigenspectrum is clustered about a point bounded away from zero, which is precisely what is required for iterative solvers, such as QMR, GMRES, and BICG, to converge.

4. Critical Mesh Spacing

In Section 3, it was illustrated how the mesh spacing plays an important role in determining the eigenspectrum of the preconditioned system. It was observed that without preconditioning, the eigenspectrum grows along the real axis as the mesh is refined. However, when the preconditioner is applied and the mesh spacing is reduced, the eigenspectrum of the preconditioned system becomes clustered about a point bounded away from zero. In the limit as $h \to 0$, the bounds for the minimum and maximum values of $\mathrm{Re}(\lambda(C^{-1}K))$ and $\mathrm{Re}(\lambda(\tilde{C}^{-1}\tilde{K}))$ indicate a tight clustering of the eigenspectrum for sufficiently small h. However, if h is chosen to be too large, the maximum and minimum real parts of the eigenvalues may become widely spread along the real axis and, in such cases, the iterative solver may be slow to converge or may not converge within a specified number of iterations. In the worst case, there may be no convergence at all. In order to overcome this, it is necessary that the mesh spacing be chosen to be sufficiently small.

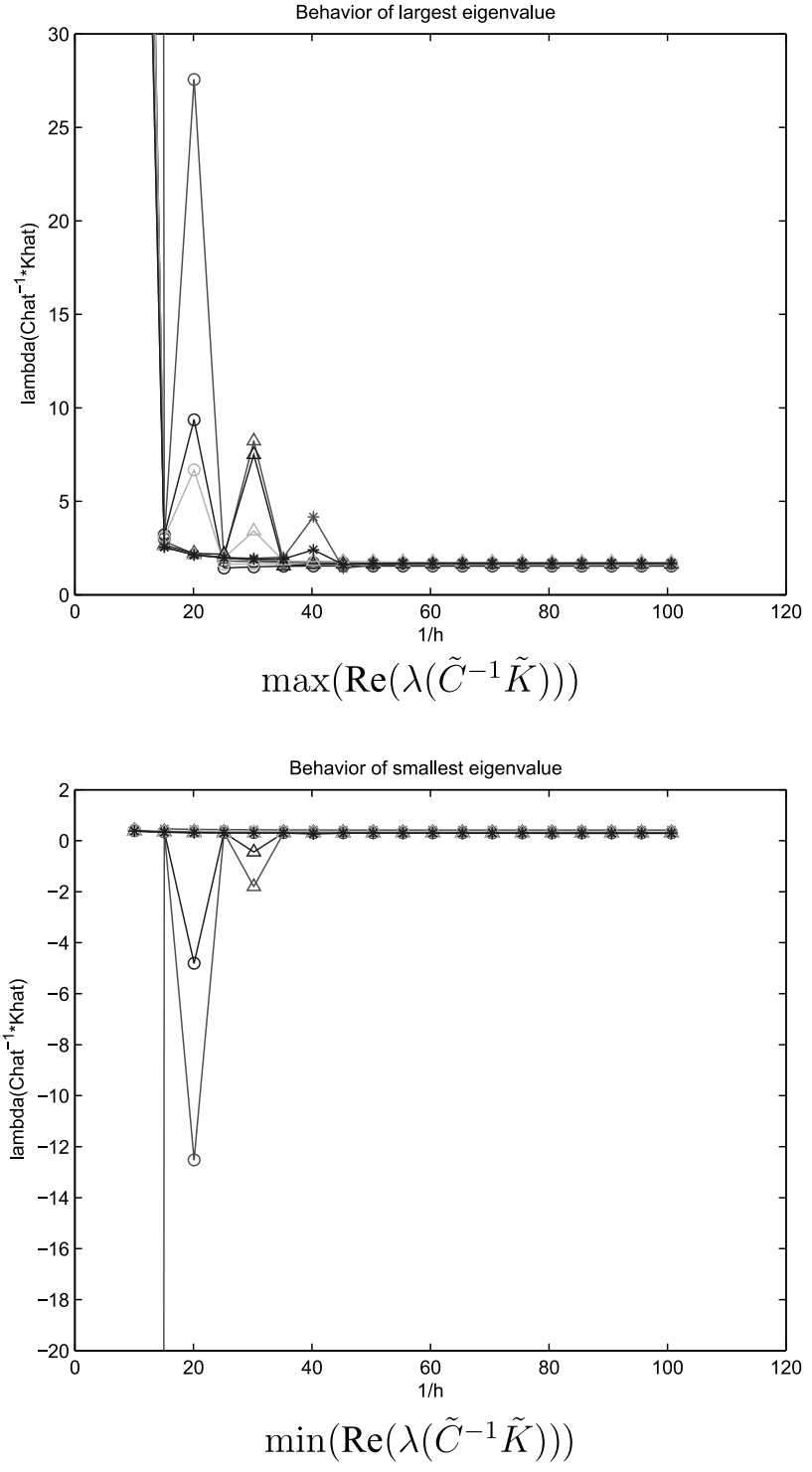

Figure 7. Behavior of $\max(\mathrm{Re}(\lambda(\tilde{C}^{-1}\tilde{K})))$ and $\min(\mathrm{Re}(\lambda(\tilde{C}^{-1}\tilde{K})))$ at discrete values of θ and ψ with h refinement.

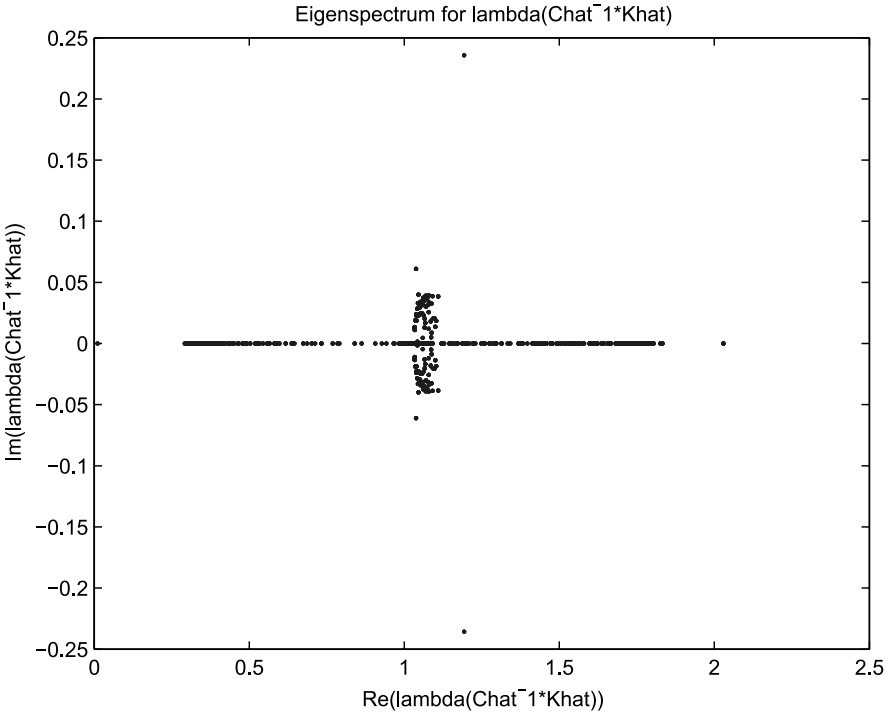

Figure 8. Eigenspectrum of $\lambda((\tilde{C}^S)^{-1}\tilde{K}^S)$ for discrete values of θ and ψ.

In Ledger (2009), a possible choice for the critical mesh spacing was outlined by appealing to the amount of numerical dispersion associated with a $p = 0$ discretization on a uniform mesh of quadrilaterals. It was proposed that h should be fine enough such that subsequent p refinement would result in exponential convergence of the solution on this mesh. The specific criteria for choosing h was based on Ainsworth's dispersion relationship for rectangular meshes of $\boldsymbol{H}(curl)$-conforming elements (Ainsworth, 2004). Discussions with Ainsworth (2008) confirmed that controlling the mesh spacing in this way is the correct approach to guarantee convergence of the iterative technique; however, the result could be stated more precisely as "h should be chosen such that $h \leq \Lambda/\pi$." For larger mesh spacings, the convergence of the preconditioned iterative solver cannot be guaranteed. The numerical results presented in the next section use this criteria to ensure convergence of the iterative solver on quadrilateral and hexahedral meshes.

Explicit formulas have been derived by Ainsworth (2004) for the numerical dispersion associated with meshes of quadrilateral and hexahedral elements of arbitrary polynomial degree, which form the basis for this choice of mesh spacing. However, the amount of numerical dispersion associated with meshes of other element types, such as triangles, depends on the shape of the element. For discretizations comprising low-order right-angled triangular elements or low-order equilateral triangular elements, explicit formulas for the numerical dispersion have also been obtained (Monk & Parrott, 1994; Monk et al., 1993). These formulas indicate that the dispersive behavior is worse than that of similarly sized quadrilaterals. Therefore, convergence of the iterative technique is unlikely for either rectangular or nonrectangular meshes with $h > \Lambda/\pi$. As a guideline, the criteria that $h < \Lambda/\pi$ is also adopted for nonrectangular meshes, although, it is possible that

in certain cases, further refinement of the mesh is necessary before convergence of the iterative solver is obtained.

5. Numerical Results

In this section, numerical results are presented to show the success of the iterative solution technique. To perform the numerical experiments, implementations of Schöberl and Zaglmayr's $\boldsymbol{H}(curl)$-conforming basis functions for triangular, quadrilateral, and hexahedral elements (Schöberl & Zaglmayr, 2005) have been undertaken. The preconditioning strategies discussed at length in Section 3 will now be tested for these elements. The specific numerical examples undertaken relate to the propagation of a plane wave in a rectangular box, which is discretized by meshes of hexahedral elements, and the scattering of the electric field by an L shaped domain, which involves a singularity at the re-entrant corner. The latter problem will be discretized by graded hybrid meshes of quadrilateral/triangular elements. The propagation of a plane wave in a rectangular box will be used to study the relative merits of the iterative solution strategies. Specifically, schemes with and without preconditioning as well as with and without static condensation will be tested. This problem will also be used to study the effect that increasing the frequency has on the performance of the preconditioned iterative solution technique. The second application will be used to show the performance of the preconditioner for a problem with a nonsmooth solution solved using nonuniform meshes.

Throughout the numerical experiments, the QMR algorithm is employed for the solution of the linear system. This is well suited to the real symmetric indefinite linear systems that arise in the numerical examples considered. However, instead of the QMR, one could use either a GMRES- or a BICG-type approach, which might give further efficiencies. No further discussion of iterative solver selection will be made in order to focus on the performance of the proposed preconditioning technique rather than the differences between the iterative solution algorithms.

5.1. *Propagation of a Plane Wave in a Cube*

The propagation of the plane wave

$$\boldsymbol{E} = \boldsymbol{p}\exp(\mathrm{i}\boldsymbol{k}\cdot\boldsymbol{x}), \qquad \text{where } \boldsymbol{p}\perp\boldsymbol{k}, \tag{26}$$

with $\omega = |\boldsymbol{k}|$ is considered across the cube $\Omega = (0,1)^3$. The material properties of Ω are $\epsilon = \mu = \mathbb{I}$ so that $\boldsymbol{E}$ satisfies $curl\, curl\, \boldsymbol{E} + \kappa \boldsymbol{E} = \boldsymbol{0}$ with $\kappa = -\omega^2$. On the boundaries of the domain, $\boldsymbol{n}\times\boldsymbol{E}$ is supplied. The domain Ω is subdivided into uniformly sized hexahedral elements. On each mesh, the polynomial degrees $p = 1, 2, 3, 4$ will be considered in turn. For the first set of results, the frequency is chosen as $\omega = 1$, and meshes with uniform spacings $h = 1, 1/2, 1/3, 1/4$ are generated. Note that the mesh spacing for each of these meshes is smaller than the critical mesh spacing $h \leq \Lambda/\pi$ for this problem.

First, the performance of the QMR for the iterative solution of the linear system without static condensation and without preconditioning is considered. Figure 9 shows the convergence of the relative residual versus the number of iterations for the different discretizations. Each subplot in this figure indicates a different mesh, and the different curves indicate different polynomial degrees. In this figure, it can be observed that the performance of iterative technique deteriorates, not only as p is increased, but also

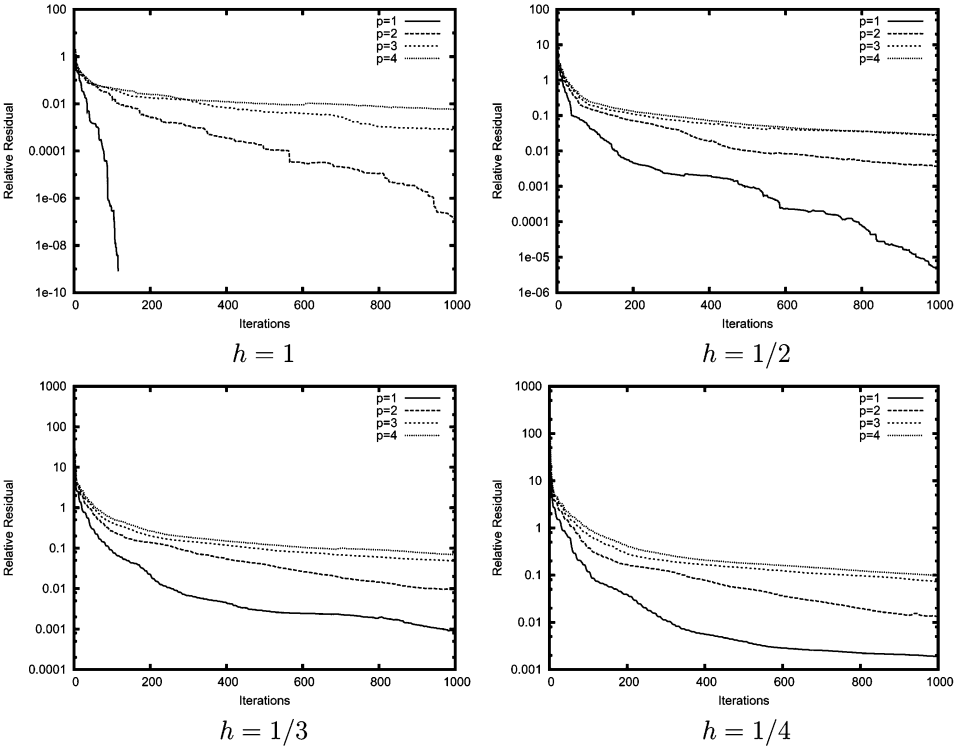

Figure 9. Propagation of a plane wave with $\omega = 1$ using discretizations with $h = 1$, 1/2, 1/3, 1/4 and $p = 1$, 2, 3, 4. Plots show the convergence of QMR for the iterative solution of the linear system without static condensation and without preconditioning.

as h is reduced. In fact, only in the cases of $p = 1$ and $h = 1$ does the iterative the solution technique actually achieve the prescribed tolerance of 10^{-9} in less than 1,000 iterations. In many cases (e.g., $p \geq 3$ for all the mesh spacing considered), the convergence behavior is very slow and appears to stagnate, indicating that for many of the discretizations considered, it is unlikely that the tolerance will ever be reached. This behavior is not unexpected. The investigation of the eigenspectrum for $p = 1$ quadrilateral elements, given in Section 3.1, predicted that the width of the eigenspectrum would grow as the mesh is refined, and consequently, the performance of an iterative solver applied to the linear system without static condensation and without preconditioning would deteriorate as the mesh is refined. Clearly, the application of the QMR without preconditioning for the linear system without static condensation is also unsatisfactory for hexahedral elements.

Second, the computations are repeated for the linear system with static condensation, but still without preconditioning. The convergence curves for this case are shown in Figure 10 and indicate an improvement over those presented in Figure 9. However, in many cases, convergence still remains slow or appears to stagnate.

Third, the calculations are repeated for the linear system without static condensation but with preconditioning. The convergence curves for this case are shown in Figure 11. The results show a clear improvement over the two previous cases (Figures 9 and 10) that had no preconditioning. For all polynomial degrees and meshes considered, the

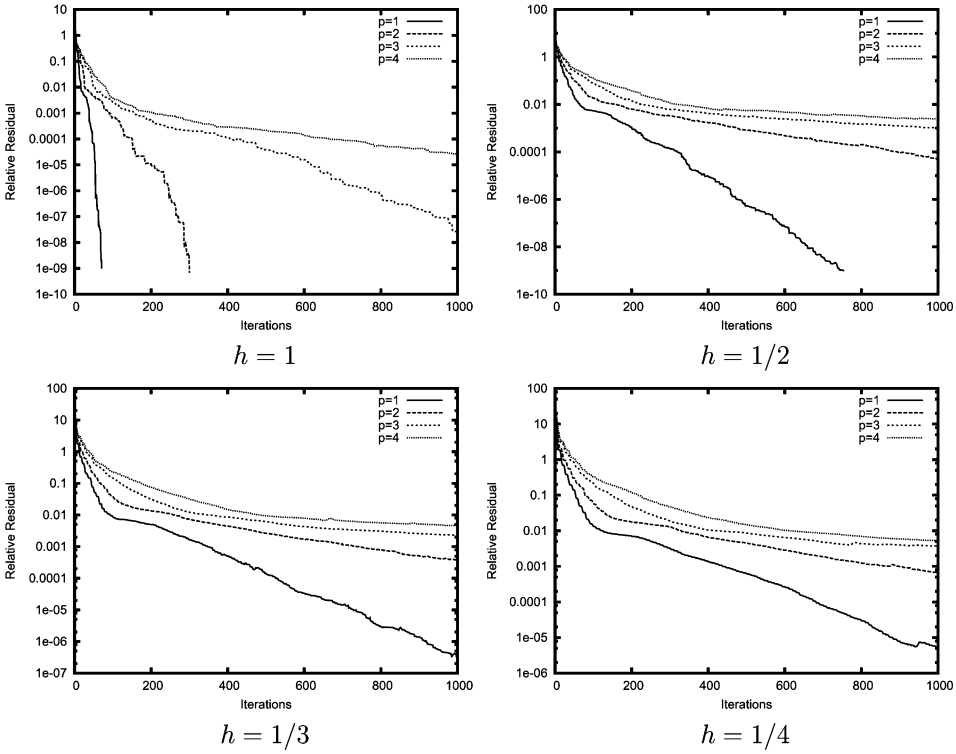

Figure 10. Propagation of a plane wave with $\omega = 1$ using discretizations with $h = 1$, 1/2, 1/3, 1/4 and $p = 1, 2, 3, 4$. Plots show the convergence of QMR for the iterative solution of the linear system with static condensation but without preconditioning.

curves indicate that the solver is converging; however, convergence is slower for high p and is not yet reached after 1,000 iterations for $p \geq 3$ on meshes with $h \leq 1/2$. Section 3.3 predicted that the maximum and minimum values of $\mathrm{Re}(\lambda(C^{-1}K))$ for $p = 1$ quadrilateral elements would become bounded for sufficiently small h and that the iterative solver applied to the preconditioned system would converge. The numerical results shown in Figure 11 illustrate that similar conclusions carry over to hexahedral elements. The notably larger numbers of iterations experienced at higher p is attributed to the large growth in the number of interior and face basis functions that are non-gradients.

Finally, the calculations are repeated for the linear system with static condensation and with preconditioning. The convergence curves for this case are shown in Figure 12. Clearly, these curves exhibit far superior convergence behavior compared to the previous three cases. The tolerance of 10^{-9} is achieved by all discretizations in less than 235 iterations. For fixed p, the growth in the number of iterations experienced when the mesh is refined is small. There is also no substantial growth in the number of iterations when the polynomial degree is increased and the mesh is kept fixed. Section 3.4 predicted that the maximum and minimum values of $\mathrm{Re}(\lambda(\tilde{C}^{-1}\tilde{K}))$ for quadrilateral elements would become bounded once the mesh spacing is sufficiently small and that performance of the iterative solver would be better with static condensation than without. This is clearly also the case also for hexahedral elements.

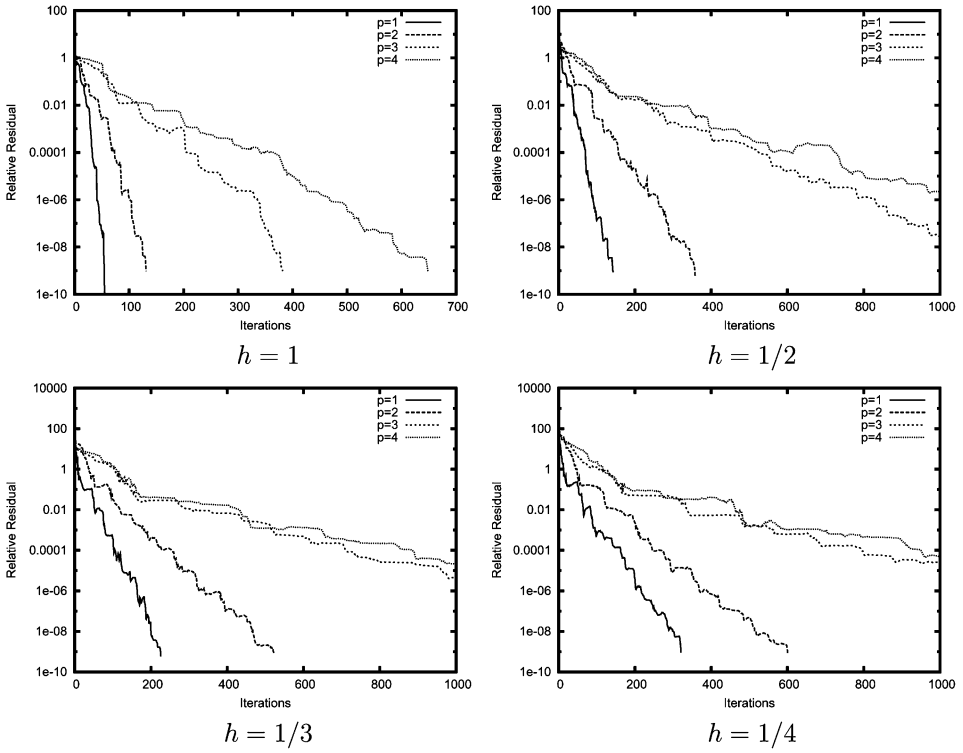

Figure 11. Propagation of a plane wave with $\omega = 1$ using discretizations with $h = 1, 1/2, 1/3, 1/4$ and $p = 1, 2, 3, 4$. Plots show the convergence of QMR for the iterative solution of the linear system without static condensation but with preconditioning.

The results presented in Figures 9, 10, 11, and 12 were for a low-frequency wave propagation problem; however, for certain practical aerospace applications (e.g., El hachemi et al., 2004), higher frequencies are of greater importance. It is clear from the previously presented results that using static condensation together with the preconditioner yielded the fewest number of iterations among the strategies investigated, and so only this approach is presented for the higher-frequency problems. To investigate the approach at higher frequencies, wave propagation problems corresponding to $\omega = \sqrt{10}$ and $\omega = 10$ are now considered. A series of four meshes of hexahedral elements are constructed for each frequency. The mesh spacings are chosen such that they are always less than or equal to the critical mesh spacing for the frequency under consideration. On each of these meshes, polynomial degrees $p = 1, 2, 3, 4$[3] are applied in turn.

The performance of the preconditioned iterative solution technique for $\omega = \sqrt{10}$ and $\omega = 10$ are shown in Figures 13 and 14, respectively. The behavior of the iterative solution technique for these two frequencies is similar to that presented in Figure 12 for $\omega = 1$. In each case, the QMR converges to the required tolerance of 10^{-9} within the specified maximum number of iterations. For a fixed value of ω, it is observed that there is virtually no increase in number of iterations when the mesh is refined and

[3]Note that the memory requirements of the discretizations $p = 4$, $h = 1/7$ and $p = 4$, $h = 1/8$ exceeded the limits of the small computer used for the numerical experiments.

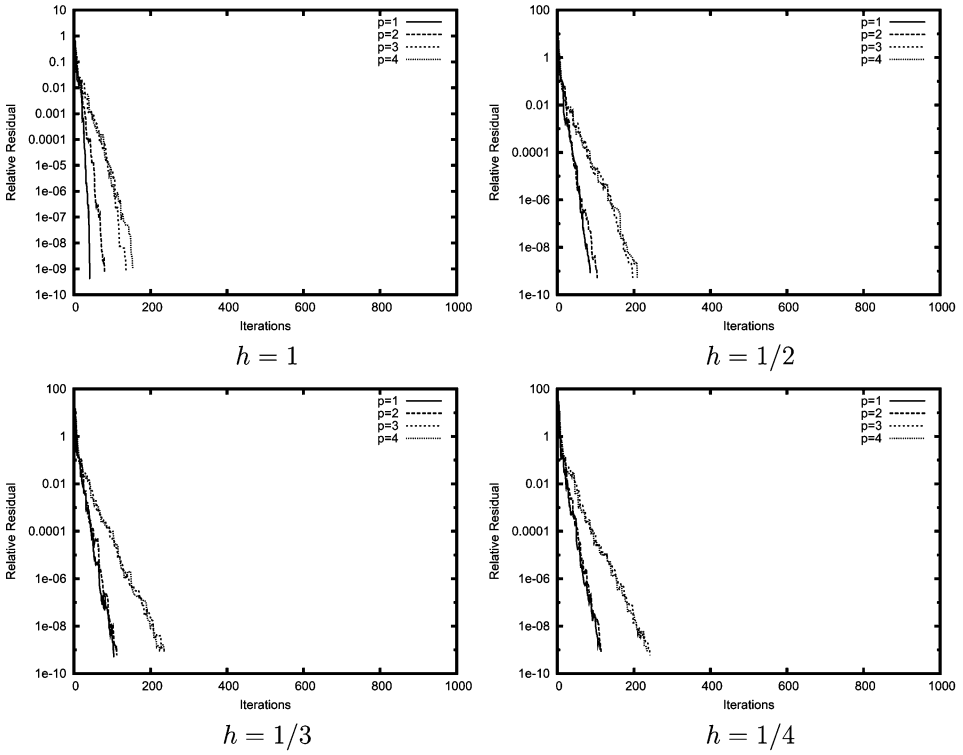

Figure 12. Propagation of a plane wave with $\omega = 1$ using discretizations with $h = 1$, 1/2, 1/3, 1/4 and $p = 1, 2, 3, 4$. Plots show the convergence of QMR for the iterative solution of the linear system with static condensation and with preconditioning.

the polynomial degree is fixed. The increase in the number of iterations observed for polynomial refinement on a fixed mesh remains small compared to the dimension of the problem. Comparing the results in Figures 12, 13, and 14, one can observe that there is increase in the number of iterations if ω is increased, even if the discretization remains the same. This behavior was not predicted in the analysis of the eigenspectrum for quadrilateral elements at small h. The difference between the numerical results and what the theory has predicted can be attributed to the fact that while the numerical experiments have confirmed that choosing $h < \Lambda/\pi$ is sufficient to ensure convergence of the scheme, using this choice of mesh spacing does not necessarily ensure that the tightest eigenvalue bounds are achieved in practice. It is conjectured that the increase in iterations can be attributed to the increase in numerical dispersion that occurs at higher frequencies (Ainsworth, 2004). It is also remarked that choosing $h < \Lambda/\pi$ alone does not ensure that dispersion is overcome, but instead that the coarse grid (i.e., using only the $\mathcal{N}_0$ basis functions) is sufficiently fine in order to ensure convergence of the iterative solver. The numerical dispersion can be exponentially reduced by combining this choice of mesh spacing with p refinement, as illustrated in the following figure.

Figure 15 shows the convergence of the error associated with the finite element approximation of the electric field $\boldsymbol{E}_H$ for $\omega = 1$, $\omega = \sqrt{10}$, and $\omega = 10$ using each of the discretizations previously discussed. The error is measured using the relative

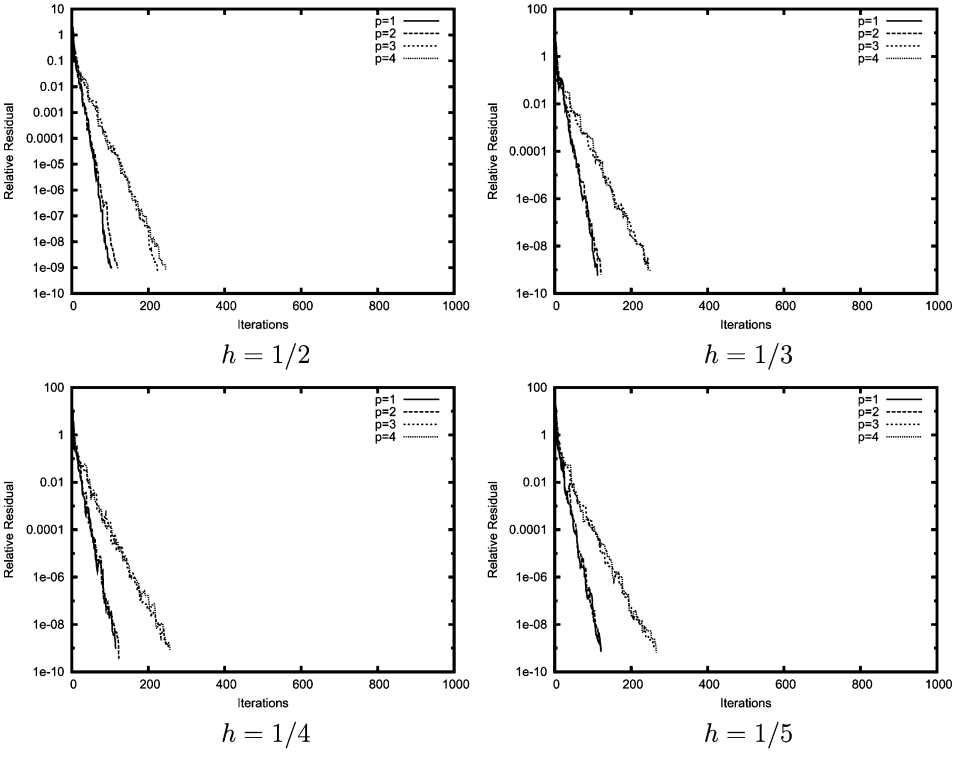

Figure 13. Propagation of a plane wave with $\omega = \sqrt{10}$ using discretizations with $h = 1/2$, 1/3, 1/4, 1/5 and $p = 1, 2, 3, 4$. Plots show the convergence of QMR for the iterative solution of the linear system with static condensation and with preconditioning.

$\boldsymbol{H}(curl)$ norm $\|\boldsymbol{E} - \boldsymbol{E}_H\|/\|\boldsymbol{E}\|$ with

$$\|\boldsymbol{u}\| = \int_\Omega |\boldsymbol{u}|^2 + |curl\, \boldsymbol{u}|^2 \mathrm{d}\Omega, \tag{27}$$

and is plotted against the total number of degrees of freedom. Each of the subplots represents a particular frequency, the different curves represent the different meshes, and the points along the curves represent increasing polynomial degree. The results in Figure 15 indicate that performing p refinement on any given mesh leads to a downward sloping curve, indicating that the convergence is exponential. This is the expected behavior for this problem (Ainsworth & Pinchedez, 2003). The set of discretizations that give rise to the lowest error for a given number of degrees of freedom corresponds to performing p refinement on the coarsest mesh.

Based on these results, the recommended solution approach for problems with smooth solutions can be summarized as follows: One should perform static condensation of the interior degrees of freedom and use a preconditioned iterative solution strategy for this system. To ensure convergence of the iterative solver, one should choose $h \leq \Lambda/\pi$. Using p refinement on the selected mesh will then lead to exponential convergence of the finite element solution when the solution is smooth. Despite the restriction on the mesh spacing imposed by the preconditioner, the iterative solution technique the

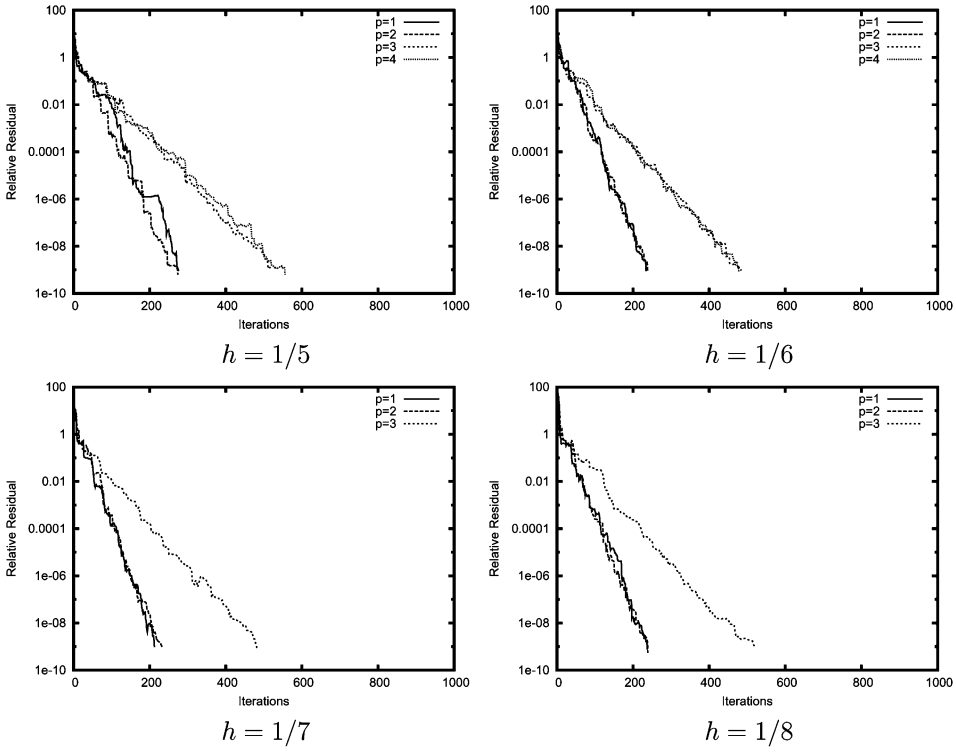

Figure 14. Propagation of a plane wave with $\omega = 10$ using discretizations with $h = 1/5$, 1/6, 1/7, 1/8 and $p = 1, 2, 3, 4$. Plots show the convergence of QMR for the iterative solution of the linear system with static condensation and with preconditioning.

scheme remains competitive and becomes more attractive as ω is increased. This is easily observed by comparing the error associated with a low-order (e.g., $p = 1$) discretization on a mesh with spacing $h = \pi/\Lambda$ as ω is increased: $\|\boldsymbol{E} - \boldsymbol{E}_H\|/\|\boldsymbol{E}\| \approx 0.5\%$ for $h = 1$ and $\omega = 1$, $\|\boldsymbol{E} - \boldsymbol{E}_H\|/\|\boldsymbol{E}\| \approx 10\%$ for $h = 1/2$ and $\omega = \sqrt{10}$, and $\|\boldsymbol{E} - \boldsymbol{E}_H\|/\|\boldsymbol{E}\| \approx$ 200 000% for $h = 1/5$ and $\omega = 10$.

5.2. *Scattering by a Re-Entrant Corner*

As a second computational test the two-dimensional model problem proposed by Ainsworth and Coyle (2001) is considered. The problem is set on an L-shaped domain that is constructed by considering the square $\Omega = (-1, 1)^2$ with the smaller square $(0, 1)^2$ removed from the bottom right-hand corner. On this domain, the electric field

$$\boldsymbol{E} = \begin{pmatrix} \partial h/\partial y \\ -\partial h/\partial x \end{pmatrix}, \qquad \text{with } h = J_\alpha(\omega r)\cos(\alpha\theta),$$

satisfies the vector wave equation $curl\, curl\, \boldsymbol{E} + \kappa \boldsymbol{E} = \boldsymbol{0}$, where $\kappa = -\omega^2$. In the above, $J_\alpha(\cdot)$ is the Bessel function of (fractional) order α, $r = \sqrt{x^2 + y^2}$, $\theta = \tan^{-1}(y/x)$ with the origin being located at the re-entrant corner. On the boundaries of the domain,

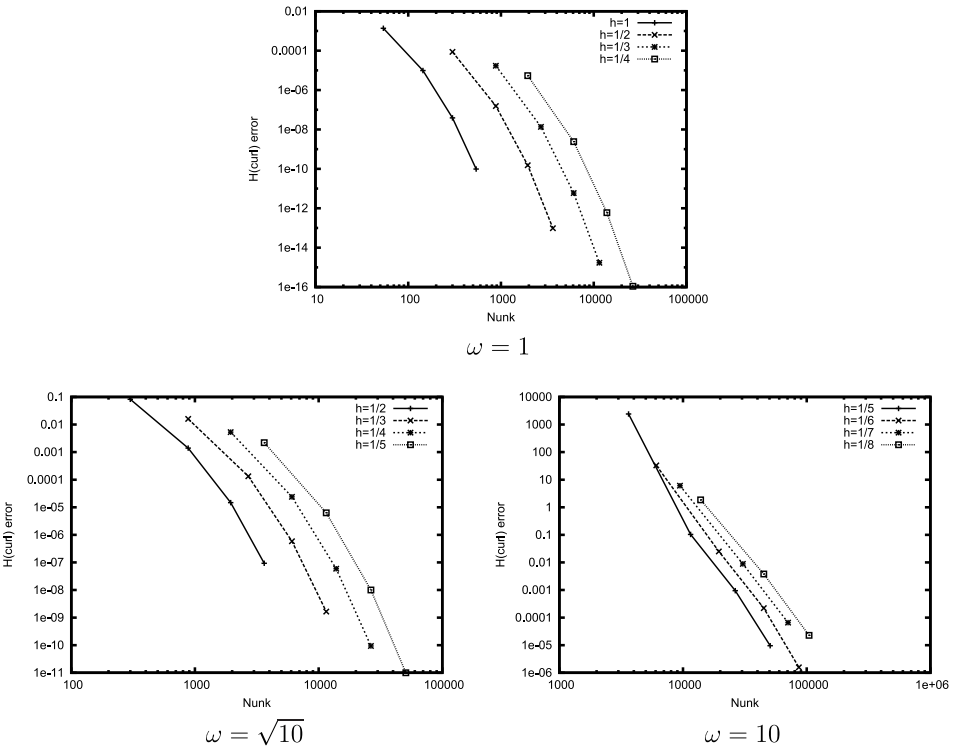

Figure 15. Propagation of a plane wave with $\omega = 1, \sqrt{10}, 10$. Plots show the convergence of the relative $\boldsymbol{H}(curl)$ norm of the error against the total numbers of unknowns.

$\boldsymbol{n} \times curl\, \boldsymbol{E}$ is specified. Depending on the order of the Bessel function, the field $\boldsymbol{E}$ may be smooth or may have a singularity at the origin. Previous experience has shown that using graded meshes and p refinement is the best approach for obtaining accurate solutions to this problem (Ainsworth & Coyle, 2001). Therefore, a series of four graded hybrid triangular/quadrilateral meshes, constructed using a grading factor of 0.5, is used for the finite element approximation of $\boldsymbol{E}$. The first two meshes in the series are shown in Figure 16. On each mesh, the uniform polynomial degrees $p = 1, 2, 3, 4, 5$ are considered in turn. The performance of the QMR for the iterative solution of the preconditioned system with static condensation is monitored for a problem with a smooth solution and for a problem where the solution contains a singularity at the origin—in the former, $\omega = \pi$ and $\alpha = 0$ and in the latter, $\omega = \pi$ and $\alpha = 2/3$. The tolerance for the relative residual is set as 10^{-9}. Note that the elements in the graded meshes are such that the largest element is always smaller than the critical spacing ($h \leq \Lambda/\pi$) for the problem under consideration.

The performance of the preconditioned iterative solution technique, when the solution is smooth, is shown in Figure 17. The results in this figure are similar to those presented for the three-dimensional wave propagation problem presented in Section 5.1 and are also similar to those presented in Ledger (2009), where meshes of uniformly sized quadrilateral elements were employed for a two-dimensional wave propagation problem. Next, the performance of the preconditioned iterative solution technique for a problem with a singularity is considered. The convergence of the relative residual for the series of

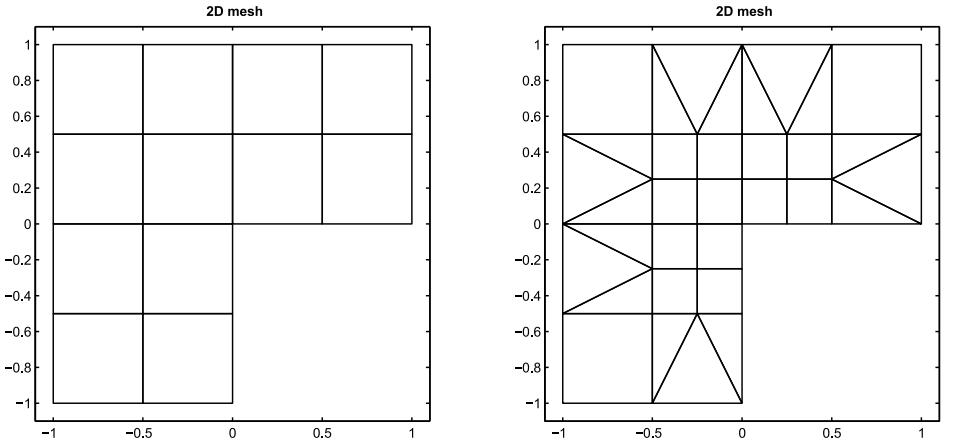

Figure 16. Scattering of the electric field $\boldsymbol{E}$ by an L-shaped domain showing the first two of a sequence of four graded meshes.

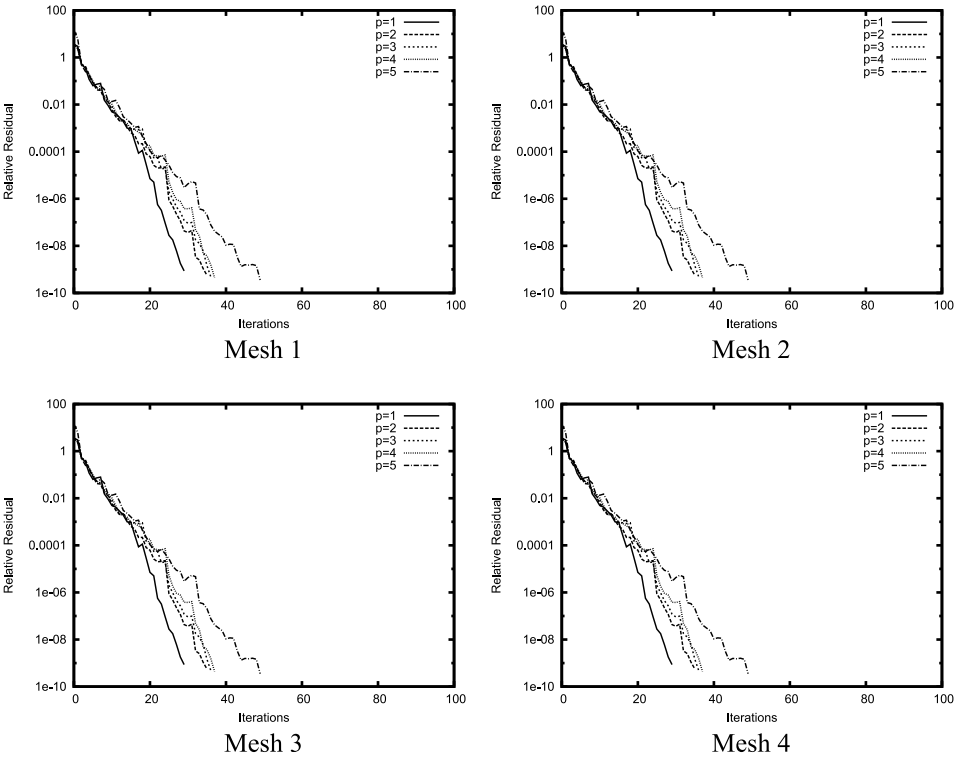

Figure 17. Scattering of the electric field $\boldsymbol{E}$ by an L-shaped domain when $\omega = \pi$ and $\alpha = 0$. Plots show the convergence of QMR for the iterative solution of the linear system with static condensation and with preconditioning.

four graded meshes is shown in Figure 18. The convergence behavior and the number of iterations required are very similar to those shown in Figure 17, indicating that the presence of a singularity in the computational domain has not adversely affected the performance of the preconditioned iterative solution technique for this problem.

The convergence of the error associated with the finite element approximation $\boldsymbol{E}_H$, measured in the relative $\boldsymbol{H}(curl)$ norm for each of the discretizations previously discussed, is shown in Figure 19. When $\alpha = 0$, the solution is smooth, and performing p refinement on the coarsest mesh yields the lowest error for a given number of degrees of freedom; for $\alpha = 2/3$, the singularity means that the lowest error for a given number of degrees of freedom is obtained by combining both h and p refinements. In both cases, the expected exponential rates of convergence (Ainsworth & Pinchedez, 2003) are observed. Moreover, the convergence of the error observed is similar to that presented by Ainsworth and Coyle (2001) for their own basis functions.

Based on these results, the recommended solution approach for problems with non-smooth solutions can be summarized as follows: One should perform static condensation of the interior degrees of freedom and use a preconditioned iterative solution strategy for this system. To ensure convergence of the iterative solver, one should ensure that the largest element in any given mesh is such that $h \leq \Lambda/\pi$. For problems with singularities, graded meshes should be used, and by combining both h and p refinements, exponential convergence of the solution can be obtained.

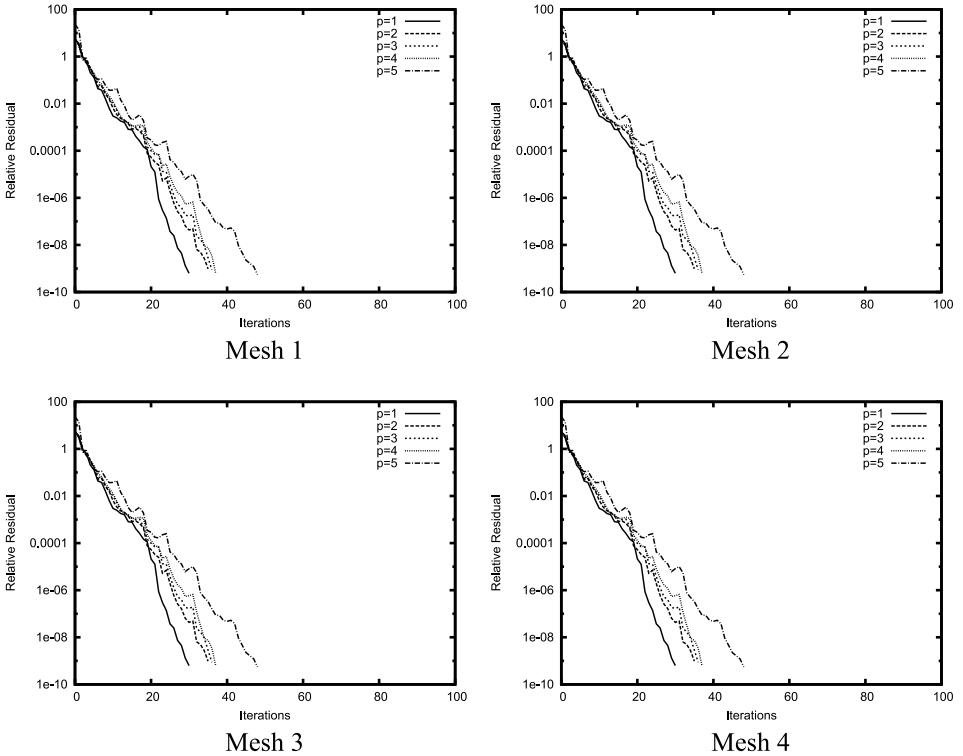

Figure 18. Scattering of the electric field $\boldsymbol{E}$ by an L-shaped domain when $\omega = \pi$ and $\alpha = 2/3$. Plots show the convergence of QMR for the iterative solution of the linear system with static condensation and with preconditioning.

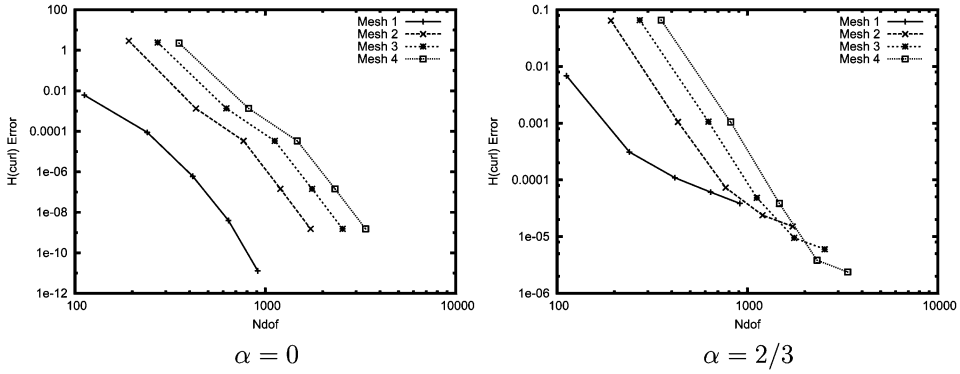

Figure 19. Scattering of the electric field $\boldsymbol{E}$ by an L-shaped domain when $\omega = \pi$ and $\alpha = 0, 2/3$. Plots show the convergence of the relative $\boldsymbol{H}(curl)$ norm of the error against the total number of unknowns.

6. Conclusion

In this article, the computational performance of a preconditioner for the indefinite system matrix obtained when the vector wave equation is discretized by the hp edge finite element proposed by Schöberl and Zaglmayr (2005) has been analyzed. The numerical results have shown that the performance of the preconditioning technique is far superior to using an iterative algorithm alone. The numerical results were justified by a theoretical investigation of the eigenspectrum of the system matrix with and without static condensation, as well as an investigation of the behavior of the eigenspectrum for the preconditioned system for $p = 1$ quadrilateral elements. The key findings were that the width of the eigenspectrum of the system matrix (with or without static condensation) grows with h refinement, which led to high numbers of iterations and slow convergence of the iterative solver. When the preconditioner is applied, the maximum and minimum real parts of the eigenvalues of the preconditioned system lie within specified bounds, once the mesh is chosen to be sufficiently fine. These bounds were found to be tighter with static condensation than without. In practical computations, this means that provided the mesh spacing is chosen to be less than the critical spacing $h \leq \Lambda/\pi$, the preconditioner will ensure that the iterative solution algorithm converges rapidly and remains robust with mesh refinement for both two- and three-dimensional problems. Despite this restriction on the mesh spacing, it was shown how the approach remains competitive, especially at higher frequencies. Ongoing work involves extending the approach to cope with varying material coefficients. Of particular interest is the application of the iterative solution technique to the case of complex-valued ϵ and μ that arise as part of the perfectly matched layer (Berenger, 1994), which is commonly used to truncate the computational domain as part of electromagnetic scattering simulations (e.g., Ledger, 2002).

Acknowledgments

The author wishes to thank the Royal Academy of Engineering for its financial support, which made his attendance at the 2008 International Workshop on Finite Element Methods in Microwave Engineering, Bonn, Germany possible. The author would also

like to thank Dr. Zaglmayr for the many interesting research discussions that were held as part of his recent visit to Graz University of Technology, Austria, which was made possible by through the support of the Royal Society. A joint paper by Dr. Zaglmayr and the author on the efficient solution of the linear system for eddy current problems on multiply connected domains is currently in preparation.

References

Ainsworth, M. 2004. Discrete properties of high order Nédélec/edge element approximation of the time-harmonic Maxwell equations. *Philosoph. Trans. Royal Soc. Ser. A* 362:471–493.

Ainsworth, M. 2008. Private communication.

Ainsworth, M., & J. Coyle. 2001. Hierarchic hp-edge element families for Maxwell's equations on hybrid quadrilateral/triangular meshes. *Comput. Methods Appl. Mechan. Eng.* 190:6709–6733.

Ainsworth, M., & J. Coyle. 2003a. Conditioning of hierarchic p version Nédélec elements on meshes of curvilinear quadrilaterial and hexahedra. *SIAM J. Numer. Anal.* 41:731–750.

Ainsworth, M., & J. Coyle. 2003b. Hierarchic finite element basis on unstructured tetrahedral meshes. *Int. J. Numer. Methods Eng.* 58:2103–2130.

Ainsworth, M., J. Coyle, P. D. Ledger, & K. Morgan. 2003. Computation of Maxwell eigenvalues using higher order edge elements. *IEEE Trans. Magnet.* 39:2149–2153.

Ainsworth, M., & K. Pinchedez. 2003. hp-approximation theory for BDRM/RT finite elements and applications. *SIAM J. Numer. Anal.* 40:2047–2068.

Arnold, D. N., R. S. Falk, & R. Winther. 2000. Multigrid in $\boldsymbol{H}(\mathrm{div})$ and $\boldsymbol{H}(curl)$. *Numer. Math.* 85:197–217.

Bayliss, A., C. I. Goldstein, & E. Turkel. 1983. An iterative method for the Helmholtz equation. *J. Computat. Physics* 49:443–457.

Beck, R., P. Deuflhard, R. Hiptmair, R. H. W. Hoppe, & B. Wohlmuth. 1999. Adaptive multilevel methods for edge element discretizations of Maxwell's equations. *Surv. Math. Indust.* 8:271–312.

Beck, R., & R. Hiptmair. 1999. Multilevel solution of the time harmonic Maxwell's equations based on edge elements. *Int. J. Numer. Methods Eng.* 45:901–920.

Berenger, J.-P. 1994. A perfectly matched layer for the absorption of electromagnetic waves. *J. Computat. Physics* 114:185–200.

Chinellato, O. 2005. *The complex-symmetric Jacobi Davidson algorithm*. Ph.D. Thesis, ETH Zurich, Switzerland.

Coyle, J., & P. D. Ledger. 2004. Evidence of exponential convergence in the computation of Maxwell eigenvalues. *Comput. Methods Appl. Mechan. Eng.* 194:587–604.

Demkowicz, L., & W. Rachowicz. 1998. *A 2D hp adaptive finite element package for electromagnetic*. TICAM Report 98-15, University of Texas at Austin.

Demkowicz, L., & L. Vardapetyan. 1998. Modeling of electromagnetic/scattering problems using hp–adaptive finite elements. *Comput. Methods Appl. Mechan. Eng.* 152:103–124.

El hachemi, M., O. Hassan, K. Morgan, D. Rowse, & N. P. Weatherill. 2004. Low order unstructured mesh approach for computational electromagnetics in the time domain. *Philosoph. Trans. Royal Soc. Ser. A* 362:445–469.

Erlangga, Y. A., C. W. Oosterlee, & C. Vuik. 2006. A novel multigrid based preconditioner for heterogeneous Helmholtz problems. *SIAM J. Sci. Comput.* 27:1471–1492.

Erlangga, Y. A., C. Vuik, & C. W. Oosterlee. 2004. On a class of preconditioners for solving the Helmholtz equation. *Appl. Numer. Math.* 50:409–425.

Erlangga, Y. A., C. Vuik, & C. W. Oosterlee. 2005. Comparison of multigrid and incomplete LU shifted-Laplace preconditioners for the inhomogeneous Helmholtz equation. *Appl. Numer. Math.* 56:648–666.

Golub, G. H., & C. F. Van Loan. 1996. *Matrix computations*, 3rd ed. Baltimore, MD: Johns Hopkins University Press.

Gopalakrishnan, J., & J. Pasciak. 2003. Overlapping Schwarz preconditioners for indefinite time harmonic Maxwell's equations. *Math. Computat.* 72:1–16.

Gopalakrishnan, J., J.E. Pasciak, & L. Demkowicz. 2004. Analysis of a multigrid algorithm for time harmonic Maxwell equations. *SIAM J. Numer. Anal.* 42:90–108.

Hiptmair, R. 1998. Multigrid method for Maxwell's equations. *SIAM J. Numer. Anal.* 36:204–225.

Karniadakis, G. E. M., & S. J. Sherwin. 1999. Spectral hp element methods for CFD. Oxford: Oxford University Press.

Laird, A. L., & M. B. Giles. 2002. *Preconditioned iterative solution of the 2D Helmholtz equation*. Report NA-02/12, Oxford University Computing Laboratory.

Ledger, P. D. 2002. *An hp-adaptive finite element procedure for electromagnetic scattering problems*. Ph.D. Thesis, University of Wales, Swansea.

Ledger, P. D. 2009. Preconditioners for the indefinite linear system arising from the hp discretisation of Maxwell's equations. *Commun. Numer. Methods Eng.* 25:275–289.

Ledger, P. D., & K. Morgan. 2005. The application of the hp-finite element method to electromagnetic problems. *Arch. Computat. Methods Sci. Eng.* 12:235–302.

Ledger, P. D., K. Morgan, & O. Hassan. 2007. Electromagnetic scattering simulation using an $\boldsymbol{H}(curl)$ conforming hp finite element method in three dimensions. *Int. J. Numer. Methods Fluids* 53:1267–1296.

Ledger, P. D., K. Morgan, O. Hassan, & N. P. Weatherill. 2002. Arbitrary order edge elements for electromagnetic scattering simulations using hybrid meshes and a PML. *Int. J. Numer. Methods Eng.* 55:339–358.

Ledger, P. D., J. Peraire, K. Morgan, O. Hassan, & N. P. Weatherill. 2003. Efficient highly accurate hp-adaptive finite element computations of the scattering width output of Maxwell's equations. *Int. J. Numer. Methods Fluids* 43:953–978.

Ledger, P. D., J. Peraire, K. Morgan, O. Hassan, & N. P. Weatherill. 2004. Parameterised electromagnetic scattering solutions for a range of incident wave angles. *Comput. Methods Appl. Mechan. Eng.* 193:3587–3605.

Monga Made, M. M. 2001. Incomplete factorization-based preconditionings for solving the Helmholtz equation. *Int. J. Numer. Methods Eng.* 50:1077–1101.

Monk, P. 2003. *Finite element method for Maxwell's equations*. Oxford: Oxford Science Publications.

Monk, P., & K. Parrott. 1994. A dispersion analysis of finite element methods for Maxwell's equations. *SIAM J. Scientif. Comput.* 15:916–937.

Monk, P., K. Parrott, & P. J. Wesson. 1993. A dispersion analysis of finite element methods on triangular grids for Maxwell's equations. *The mathematics of finite elements and applications*, 315–321, J. R. Whiteman, ed. Chichester: John Wiley and Sons Ltd.

Nédélec, J. C. 1978. Computation of eddy currents on a surface in $\mathbb{R}^3$ by finite element methods. *SIAM J. Numer. Anal.* 15:580–594.

Nédélec, J. C. 1980. Mixed elements in $\mathbb{R}^3$. *Numer. Math.* 35:315–341.

Nédélec, J. C. 1986. A new family of mixed elements in $\mathbb{R}^3$. *Numer. Math.* 50:57–81.

Pardo, D., L. Demkowicz, & J. Gopalakrishnan. 2006. Integration of hp-adaptivity and a two grid solver for electromagnetic problems. *Comput. Methods Appl. Mechan. Eng.* 195:2533–2573.

Rachowicz, W., & L. Demkowicz. 2002. A three-dimensional hp adaptive finite element package for electromagnetics. *Int. J. Numer. Methods Eng.* 53:147–180.

Saad, Y. 1996. *Iterative methods for sparse linear systems*, 1st ed. Available at http://www-users.cs.umn.edu/∼ saad/books.html (Y. Saad website).

Schöberl, J., & S. Zaglmayr. 2005. High order Nédélec elements with local complete sequence properties. *Int. J. Computat. Math. Elect. Electron. Eng. (COMPEL)* 24:374–384.

Schwab, Ch. 1998. *p and hp finite element methods. Theory and applications in solid and fluid mechanics*. Oxford: Oxford Science Publications, Clarendon Press.

Strang, G. 1976. *Linear algebra and its applications*. New York: Academic Press.

Strang, G., & G. J. Fix. 1973. *An analysis of the finite element method*. London: Prentice Hall.

Zaglmayr, S. 2006. *High order finite element methods for electromagnetic field computation*. Ph.D. Thesis, Institut für Numerische Mathematik, Johannes Kepler Univerität, Linz, Austria.